Gibberellin and abscisic acid transporters facilitate endodermal suberin formation in *Arabidopsis*

Jenia Binenbaum
Tel Aviv University
Nikolai Wulff
https://orcid.org/0000-0002-7524-104X
Lucie Camut
Université de Strasbourg
Kristian Kiradjiev
University of Nottingham
Iris Tal
Tel Aviv University
Himabindu Vasuki
Weizmann Institute of Science https://orcid.org/0000-0002-7106-3506
Moran Anfang
Tel Aviv University
Yuqin Zhang
Tel Aviv University
Lali Sakvarelidze-Achard
Institut de biologie moléculaire des plantes, CNRS, Université de Strasbourg
Jean-Michel Davière
IBMP-CNRS
Dagmar Ripper
ZMBP-Center for Plant Molecular Biology, University of Tübingen
Esther Carrera Bergua
IBMCP-UPV
Ekaterina Manasherova
Volcani Center
Shani Lazary
Tel Aviv University
Vlastimil Novak
University of Copenhagen https://orcid.org/0000-0001-7890-4593
Christoph Crocoll
University of Copenhagen https://orcid.org/0000-0003-2754-3518
Roy Weinstein

Department of Molecular Biology and Ecology of Plants, Tel Aviv University

Hagai Cohen

Volcani Center

Laura Ragni

ZMBP-Center for Plant Molecular Biology, University of Tübingen https://orcid.org/0000-0002-3651-8966

Asaph Aharoni

Weizmann Institute of Science https://orcid.org/0000-0002-6077-1590

Leah Band

University of Nottingham

Patrick Achard

Institut de biologie moléculaire des plantes, CNRS, Université de Strasbourg https://orcid.org/0000-0003-0520-7839

Hussam Nour-Eldin

Copenhagen University https://orcid.org/0000-0001-6660-0509

Eilon Shani (eilonsh@tauex.tau.ac.il)

Tel Aviv University https://orcid.org/0000-0002-1262-350X

Article

Keywords:

Posted Date: May 25th, 2022

DOI: https://doi.org/10.21203/rs.3.rs-1670556/v1

Version of Record: A version of this preprint was published at Nature Plants on April 6th, 2023. See the published version at https://doi.org/10.1038/s41477-023-01391-3.

Abstract

The plant hormone gibberellin (GA) regulates multiple developmental processes. It accumulates in the root elongating endodermis, but how it moves into this cell file and the significance of this accumulation are unclear. Here, we identified a monophyletic clade of NPF transporters required for GA and abscisic acid (ABA) translocation. We demonstrate that NPF2.14 is a subcellular GA/ABA transporter, the first to be identified in plants, facilitating GA and ABA accumulation in the root endodermis to regulate suberization. Further, NPF2.12 and NPF2.13, closely related proteins, are plasma membrane-localized GA and ABA importers that facilitate shoot-to-root GA_{12} translocation, regulating endodermal hormone accumulation. This work reveal that GA promotes root suberization and that GA and ABA can act non-antagonistically. We demonstrated how a clade of transporters mediates hormone flow while utilizing defined cell-file-specific vacuolar storage at the phloem unloading zone, allowing a hormone slow-release mechanism required for suberin formation in the maturation zone.

Introduction

The phytohormone gibberellin (GA) is essential for many developmental processes in plants. Among them are seed germination, organ elongation and expansion through cell growth and division, trichome development, the transition from vegetative to reproductive growth, and flower, seed, and fruit development [1]. GAs are produced mainly in the vasculature and move long distances in both acro- and basipetal directions [2–5]. The first reports of GA mobility through the phloem sap appeared over 50 years ago [6–8]. Grafting methods showed that biosynthesis of GA in the shoot can rescue GA biosynthesis mutations in the hypocotyl and root and *vice versa* [6–8]. In tobacco plants, defoliation results in an internode elongation, cambial activity, and fiber differentiation phenotypes that are similar to treatment with paclobutrazol, a GA biosynthesis inhibitor [5]. Another example of an organ dependent on an external source of GA are the petals, which require the anthers as their GA source [9,10]. The biosynthesis of active GA is a complex, multi-step process with diverse intermediates [11]. Regnault et al. conducted a series of grafting experiments using *Arabidopsis thaliana* mutant plants compromised at different stages of GA biosynthesis and identified GA_{12} as the major GA form transported over a long distance through the vasculature [12]. GA_{12} moves through the xylem in a root-to-shoot manner and in the phloem in a shoot-to-root direction to regulate plant growth [12]. The translocation of GA_{12} from the root to the shoot is enhanced under ambient temperatures to induce shoot growth [13]. The transporters that regulate GA long-distance transport in the plant remain unknown.

In recent years, a number of *Arabidopsis* GA plasma membrane transporters have been identified, two from the SWEET family and several others from the NITRATE TRANSPORTER1/PEPTIDE TRANSPORTER (NPF) family [14–17]. There are 53 NPFs in *Arabidopsis*, divided into eight subfamilies. These proteins are capable of transporting a large variety of substrates such as nitrate, glucosinolates, abscisic acid (ABA), auxin, and GAs [14,18,19]. Like auxin, GA is subjected to the ion-trap mechanism, limiting its ability to move

out of cells. The existence of GA efflux transporters is therefore predicted to allow GA cell-to-cell movement [20]; however, no GA efflux transporters have been discovered [21].

ABA, which regulates growth and stress responses, has been long thought to act antagonistically to GA in processes such as seed germination, seed maturation, and dormancy and in responses to external cues [22–24]. Both GA and ABA induce developmental responses specifically from the endodermis [25–27]. GA accumulates at high levels in the endodermal cells of the root elongation zone [28]. The process is dependent on the activity of NPF3.1 (NPF3), a member of the NPF family, which has been shown to act as a dual-specificity GA and ABA importer [16,29]. The endodermis, the innermost cortical layer that surrounds the central vasculature, goes through two phases of differentiation: The first step involves polar localized lignin deposition, which results in the formation of the casparian strips, and the second is the deposition of suberin as a lamella below the primary cell wall [30]. The casparian strips restrict apoplastic diffusion of water and nutrients into the vascular tissues, whereas suberin limits backflow of nutrients from the stele [31,32]. The physiological relevance of GA accumulation in the endodermis remains unknown.

With this study, we identified a monophyletic clade of NPF transporters that orchestrate GA_{12} long-distance shoot-to-root translocation and promote bioactive ABA and GA movement from the vasculature to the endodermis, which is required for endodermal suberization, a phenotype rescued by applying either ABA or GA. The importance of transporter distributions was evaluated via a multicellular mathematical model that revealed an intriguing slow-release mechanism wherein high levels of GA and ABA in the phloem unloading zone are loaded into pericycle vacuoles for continued induction of suberin formation in the maturation zone. Together, our findings reveal the mechanism that facilitates long-distance shoot-to-root movement of GA_{12} and explain how bioactive GA_4 and ABA are transported from the vasculature to the endodermis to mediate endodermal suberization.

Results

NPF2.14 is a tonoplast-localized GA and ABA transporter

To identify the missing GA exporters in plants, we tested whether NPF proteins were capable of GA_4 export in *Xenopus laevis* oocyte-based transport assays. Other GA transporters identified to date import GA [14,33]. The transport assays investigate whether NPFs lead to efflux of GA that is loaded into oocytes by three different approaches, namely diffusion, injection and import by a GA importer. Oocytes expressing various *NPFs* or control oocytes injected with water were exposed to an array of membrane-permeable GAs (GA_4, GA_7, GA_9 and GA_{12}) [34]. The screen has identified NPF2.14 as a potential GA exporter. At the end of assay, NPF2.14-expressing oocytes contained significantly reduced GA levels compared to control oocytes (Fig. 1A). This suggests that NPF2.14 facilitates the export activity of GAs out of oocytes. This was confirmed in an injection-based assay in which GA_3, a non-membrane-permeable form of GA, was injected directly into the oocyte. At the end of the assay, there was a lower

GA_3 content in NPF2.14-expressing oocytes compared to control oocytes (Fig. 1B). Co-expression of both *NPF2.14* RNA and *NPF4.1*, which encodes a known GA importer, led to a reduced accumulation of non-membrane permeable GA_3 compared to oocytes expressing only *NPF4.1* (Fig. 1C), further supporting that NPF2.14 exports GA out of *Xenopus laevis* oocytes.

It was previously shown that NPF3.1 transports both GA and ABA in *Xenopus laevis* oocytes [16]. To test whether NPF2.14 also has broad substrate specificity, control and NPF2.14-expressing oocytes were exposed to ABA. NPF2.14-expressing oocytes accumulated less ABA than did control oocytes (Fig. 1D), indicating that NPF2.14 has dual-substrate transport activity. Several NPF transporters, including NPF6.3, also transport nitrate [18], but NPF2.14 displayed no nitrate transport activity in oocyte assays (Fig. 1E).

Wulff et al. recently showed that NPF7.3 lowers the cytoplasmic pH in *Xenopus laevis* oocytes, which can indirectly influence the accumulation equilibrium of weak acids such as GA and ABA [34]. In order to assess whether NPF2.14 has a similar activity, we measured the intracellular oocyte pH using a proton-selective three-electrode voltage clamp setup. We showed that, unlike NPF7.3, NPF2.14 expression in the oocyte does not alter the internal oocyte pH (Fig. 1F). Another factor that theoretically can lead to a false-positive GA export result is alteration of membrane potential. Therefore, we measured the membrane potential of control and NPF2.14-expressing oocytes using a two-electrode voltage clamp setup. The membrane potential of control and NPF2.14-expressing oocytes were both approximately − 15 mV (Fig. 1G). When oocytes were subjected to GA_4 for 60 min prior to membrane potential measurement, less GA was observed in NPF2.14-expressing oocytes than control oocytes (Fig. 1G). Thus, NPF2.14 does not shift oocyte membrane potential.

Many NPF proteins, including NPF2.14, contain the ExxE[K/R] motif [35], which is involved in coupling substrate transport to the proton gradient across membranes [36]. Involvement of the ExxE[K/R] motif in NPF2.14-mediated effluxes would suggest antiporter function. To assess the involvement of the ExxE[K/R] motif, we generated C-terminal YFP-tagged NPF2.14 mutants substituted at each of the three charged residues with a polar but uncharged residue. The YFP-tag alone did not influence the apparent GA_4 transport by the wild-type NPF2.14 (Fig. 1H). When any of the charged residues of the ExxE[K/R] motif were replaced with the polar uncharged Gln residue, no significant difference in GA_4 transport was observed compared to wild-type NPF2.14 (Fig. 1H). Thus, the GA_4 transport mediated by NPF2.14 seems to be ExxE[K/R] motif independent.

In order to test whether the *Xenopus laevis* oocyte GA transport data is physiologically relevant *in planta*, we isolated a homozygous T-DNA knockout line for *NPF2.14*. The single *npf2.14* mutant did not show significant shoot or root growth phenotypes (**Sup. Figure 1A-C**). Several NPF family members transport nitrate, including NPF6.3 [37]. Thus, despite having shown that NPF2.14 does not transport nitrate in oocytes (Fig. 1D), we checked whether *npf2.14* mutants display an impaired growth on low nitrate media. *npf2.14* T-DNA insertion mutants did not have a visible growth phenotype and did not differ from Col-0 plants under low nitrate conditions (**Sup. Figure 1D**). To determine whether NPF2.14 is involved in GA

distribution and accumulation in the root, we tested whether the distribution of a fluorescently tagged GA_3 compound (GA_3-Fl) was affected in the loss-of-function line. GA_3-Fl has been developed in our lab to serve as a stable, bioactive reporter to study GA movement/accumulation *in planta* [28]. Accumulation of GA3-Fl in the endodermis was visible in the Col-0 plants, as previously shown [25]. The *npf2.14* mutants displayed a significantly stronger signal compared to the Col-0 control (Fig. 1I). This enhanced accumulation was restored to normal levels when expressing *NPF2.14* driven by its native promoter (*pNPF2.14:NPF2.14-GFP*) on the background of the *npf2.14* T-DNA line (Fig. 1I), indicating that loss of NPF2.14 affects GA3-Fl distribution in the plant. In agreement with this result, *npf2.14* mutants accumulated significantly higher levels of GA_4 in their roots (Fig. 1J).

In order to study the subcellular localization of NPF2.14, we generated and imaged *35S:NPF2.14-YFP* lines. Interestingly, NPF2.14 localized to the tonoplast vacuole membrane (Fig. 1K). Therefore, although we had hypothesized that NPF2.14 was a GA exporter that transported GA from inside the cytosol to the apoplast, the protein is instead a tonoplast-localized transporter. To the best of our knowledge, this is the first report of a sub-cellular GA/ABA transporter.

NPF2.14 regulates suberin formation in the root endodermis

To characterize NPF2.14 expression patterns in the plant, we generated NLS-YFP and GUS reporter lines driven by the *NPF2.14* promoter. Confocal imaging of the NLS-YFP lines indicated that NPF2.14 is expressed only in the pericycle of the root mature zone, mainly in the phloem poles, and not in the meristematic zone (**Fig. 2A, Sup. Fig. 2A**). In addition, GUS staining showed expression in the shoot vasculature in seedlings (**Sup. Fig. 2B**). In the mature stages, the *NPF2.14*-driven reporter was expressed in the periderm (**Sup. Fig. 2C**). The pericycle is a deep layer of post-embryonic meristematic cells encircling the vascular tissue [38]. In the root, it is required for lateral root emergence [39], xylem loading [40] and phloem unloading [41]. Later stages give rise to the periderm, which serves as the outer protective layer when the surrounding tissue is sloughed off [38]. Both the pericycle and the cork, which is the outermost cell layer of the periderm are suberinized tissues [42].

The expression of the reporter driven by the *NPF2.14* promoter in tissues that undergo suberization, taken together with the ability of NPF2.14 to transport ABA, which has been previously shown to regulate root suberization [43], led us to hypothesize that this transporter might facilitate root suberization.

To test this, we analyzed suberization in *npf2.14* T-DNA mutants using Nile red and Fluorol yellow, which are suberin dyes [44,45]. Suberization commences in the endodermis of the upper part of the maturation zone of the root, and, as the plant matures more cells undergo suberization [46]. Quantification of Nile red and Fluorol yellow fluorescence intensity in the uppermost part of 5-day-old roots revealed that the mutant *npf2.14* plants had significantly lower levels of endodermal suberization than Col-0 plants (**Fig. 2B, Sup. Fig. 3**).

Suberin is a complex polyester based on glycerol and long-chain α,ω-diacids and ω-hydroxyacids [47], which is primarily found in structures such as the periderm, endodermis, and seed coat [30]. To examine changes in root suberin composition between *npf2.14* and Col-0, we analyzed their suberin monomer profiles via gas chromatography-mass spectrometry (GC-MS). We found significant reductions in ferulic acid, the predominant aromatic component of suberin, as well as in C22 fatty acid and C18:1(9) ω-hydroxyacid, two of the most abundant suberin building blocks in the Arabidopsis root endodermis (**Fig. 2C**). In addition, C18 ester was lower in *npf2.14* roots. These reductions accompanied by lower levels of other monomers resulted in 35% less total suberin contents in the mutant roots (**Fig. 2C**). Overall, the findings provide several lines of evidence that alteration of NPF2.14 has a substantial effect on suberin deposition in the root endodermis.

Similar to the *npf2.14* mutant, *npf3.1* mutant plants, which have been shown to have impaired GA and ABA delivery to the endodermis [16], displayed reduced suberization levels compared to Col-0 plants (**Sup. Fig. 4**). GA and ABA treatments completely rescued the *npf2.14* mutant suberization levels (**Fig. 2B**).

Endodermal suberization is regulated by ABA perception, both under normal and stress conditions [43,48]. ABA treatment was previously reported to induce endodermal suberization [49]. In agreement with this report, ABA significantly upregulated the Nile red fluorescence intensity in the root endodermis and rescued the reduced suberization observed in the *aba2-1* mutant, which is deficient in ABA biosynthesis [49] (**Fig. 2D**). To the best of our knowledge, GA has not been previously associated with endodermal suberization. To establish whether or not GA regulates root suberization in *Arabidopsis* seedlings, we quantified suberization levels in GA-treated wild-type and *ga1-13* mutant plants using Nile red and Fluorol yellow dyes. GA1 catalyzes the first committed step in the GA biosynthetic pathway [50]. GA treatment to wild-type caused significant induction in endodermal root suberization (**Fig. 2E, Sup. Fig. 5**), and the GA biosynthesis mutant *ga1-13* displayed a significant reduction in suberization levels, which was restored by the exogenous application of GA_3 (**Fig. 2E)**. GA and ABA have long been thought to have completely antagonistic functions [51]. Our results indicate that this antagonistic activity is more complex and that GA and ABA enhance root suberization. Taken together, our data suggest that NPF2.14 is a pericycle-specific GA and ABA transporter, localized to the tonoplast, and involved in regulating GA and ABA accumulation in the endodermis to promote suberization.

NPF2.12 and NPF2.13 are plasma membrane-localized GA and ABA importers

NPF2.12 and its close paralog *NPF2.13* form a monophyletic phylogenetic clade with *NPF2.14* (**Fig. 3A, Sup. Fig. 6**). We hypothesized that due to this proximity on the phylogenetic tree, NPF2.12 and NPF2.13 might also contribute to GA and ABA accumulation in the endodermis. Both transporters were previously characterized as low-affinity nitrate transporters [52,53] and more recently, were shown to promote GA import activity in heterologous systems [14,34]. Neither have been characterized in plants as GA or ABA transporters. To test for direct GA transport activity of NPF2.12 and NPF2.13, we performed *Xenopus laevis* oocyte-based transport assays. Oocytes expressing NPF2.12 or NPF2.13 accumulated significantly

higher levels of GA_1, GA_3, GA_4, GA_7, GA_9, GA_{12}, GA_{19}, and GA_{24} compared to control oocytes over the course of 60 min (**Fig. 3B, Sup. Fig. 7A**). This suggests that NPF2.12 and NPF2.13 are promiscuous GA transporters. Both NPF2.12- and NPF2.13-expressing oocytes also had higher levels of ABA accumulation than controls (**Fig. 3C**).

NPF2.12 and NPF2.13 both contain an ExxE[K/R] motif, which couples the substrate transport to the proton gradient [36]. To test whether NPF2.12 and NPF2.13 substrate transport activity is coupled with external proton concentration, NPF2.12- and NPF2.13-expressing oocytes were treated with membrane-impermeable GA_1 in solutions ranging from pH 5 to 7 in 0.5 pH unit increments. In both NPF2.12- and NPF2.13-expressing oocytes, GA_1 accumulation increased as pH was lowered. (**Fig. 3D**). These data indicate that GA transport by NPF2.12 and NPF2.13 is likely proton-coupled.

Proton-coupled transport is electroneutral if the proton-to-substrate stoichiometry is 1:1. To investigate whether the transport of GA by NPF2.12 and NPF2.13 is electrogenic, we used two-electrode voltage clamp electrophysiology to evaluate oocytes that express the transporters. Subtracting the currents elicited by oocytes at different membrane potentials in the absence of GAs from the currents elicited by oocytes in the presence of 500 µM GA_3 revealed that GA_3 transport by both NPF2.12 and NPF2.13 is associated with negative currents relative to control oocytes (**Fig. 3E**). The negative currents reflect a net positive influx of charges through both NPF2.12 and NPF2.13 upon GA_3 exposure. At low negative membrane potential (-20 mV), GA_3-induced currents in NPF2.12-expressing oocytes were of the same magnitude as those of control oocytes, whereas at high negative membrane potential (-120 mV), GA_3 induced-currents in NPF2.12-expressing oocytes were of the same magnitude as those of NPF2.13-expressing oocytes (**Fig. 3E, F**). This suggests that the apparent higher uptake of GA by NPF2.13 compared to NPF2.12 (**Fig. 2B**) likely reflects the membrane potential of resting *Xenopus* oocytes. In agreement with previous publications [52,53], we detected nitrate import into oocytes that expressed NPF2.12 or NPF2.13, but this transport did not interfere with the GA transport capabilities as GA accumulation was not affected in GA/nitrate competition assays (**Sup. Fig. 7B**).

To elucidate whether these transporters are part of the GA transport mechanisms in the plant, we treated T-DNA knockout lines, which did not display any visible phenotypes (**Sup. Fig. 8**), with GA_4-Fl. *npf2.12* and *npf2.13* single mutant plants treated with GA_4-Fl displayed a significant reduction in accumulation in the endodermis compared to Col-0 plants (**Fig. 3G**), similar to reduced levels detected in *npf3.1* mutants. To verify that the reduction in GA-Fl accumulation was not due to an off-target mutation, we repeated the test with an additional *npf2.12* T-DNA insertion line (*npf2.12-2*) and obtained similar results (**Sup. Fig. 9A**). In addition, homozygous *pNPF2.13:NPF2.13-YFP* plants completely rescued the root GA_3-Fl phenotype (**Sup. Fig. 9B**).

We next generated plants ectopically expressing *NPF2.12* and *NPF2.13* fused to YFP (*p35S:NPF2.12-YFP* and *p35S:NPF2.13-YFP,* respectively) and treated them with GA_3-Fl. These lines showed a remarkably strong accumulation of GA_3-Fl in all root cells (**Fig. 3H**), supporting the hypothesis that NPF2.12 and

NPF2.13 are GA transporters *in planta*. In order to test whether NPF2.12 and NPF2.13 have a dual specificity function and can also import ABA, we treated plants with fluorescently tagged ABA (ABA-Fl). ABA-Fl is non-bioactive but can be utilized to estimate ABA movement in the plant [33]. Overexpression of NPF2.12 or of NPF2.13 resulted in extreme ABA-Fl accumulation compared to Col-0 plants (**Fig. 3H**), implying that both transporters import GA and ABA *in planta*.

In order to address the subcellular localization of NPF2.12 and NPF2.13, we imaged the root epidermis cells of *p35S:NPF2.12-YFP* and *p35S:NPF2.13-YFP* lines. Both NPF2.12 and NPF2.13 are localized to the plasma membrane (**Fig. 3I**). Together, the *in planta* and oocyte results indicate that NPF2.12 and NPF.13 are dual-substrate, plasma membrane-localized GA and ABA importers.

NPF2.12 and NPF2.13 regulate root suberization

To further elucidate the biological function of NPF2.12 and NPF2.13, we generated NLS-YFP and GUS reporter lines to map NPF2.12 and NPF2.13 expression patterns. Confocal microscopy of plants expressing *NLS-YFP* driven by *NPF2.12* and *NPF2.13* native promoters revealed that in the root, NPF2.12 was expressed in the pericycle of the whole root and subsequently in the periderm of mature plants; NPF2.13, on the other hand, was expressed only in the shoot (**Fig. 4A, Sup. Fig. 10**). Analysis of *pNPF2.12:GUS* and *pNPF2.13:GUS* lines showed that the two transporters are expressed in the shoot vasculature (**Fig. 4B)**. The fact that the *NPF2.13* translational fusion construct (*pNPF2.13*:*NPF2.13-Venus)* introduced into the *npf2.13* mutant background rescued the root GA_3-Fl accumulation phenotype indicated that the promoter region we cloned is sufficient and that NPF2.13 expression is restricted to the shoot (**Sup. Fig. 9B**).

Similar to *npf2.14* mutants, *npf2.12* and *npf2.13* mutant plants displayed a reduction in suberization. Mutant roots stained with Nile red or Fluorol yellow showed a weaker fluorescence intensity than detected in Col-0 plants (**Fig. 4C, Sup. Fig. 11**). Similar results were obtained using additional mutant alleles for *npf2.12* and *npf2.13* (**Sup. Fig. 12**). The phenotype was enhanced in the *npf2.12 npf2.13* double mutant line (**Fig. 4C**). Notably, GA_3 or ABA treatment completely rescued *npf2.12* low-suberin phenotype. The phenotypes of *npf2.13* and of the *npf2.12 npf2.13* double mutant were completely rescued by ABA and largely rescued by GA_3 (**Fig. 4C**). Quantification of suberin monomer content revealed that both *npf2.12* and *npf2.13* mutant roots accumulated ~40% less total suberin contents compared to the Col-0 attributed to lower levels of vanillic and ferulic acids, C22 fatty acid, C20 fatty alcohol, and C18:1(9), C22 and C26 -hydroxyacids (**Fig. 4D**).

NPF2.12 and NPF2.13 regulate shoot-to-root GA translocation

Our previous work showed that GA_{12}, though not bioactive, is the primary GA form transported over long distances through the vasculature in *Arabidopsis thaliana* [12]. GA_{12} can move through the xylem in a root-to-shoot manner and in the phloem in a shoot-to-root direction to regulate adaptive plant growth [12,13]. However, the mechanism regulating this process remains unknown [21]. NPF2.13 was expressed strictly in

the shoot (**Fig. 4A, B**), yet the knockout led to a phenotype in the root endodermis (**Fig. 4C**). This led us to hypothesize that the transporters are involved in the long-distance shoot-to-root translocation of GA. To test whether NPF2.12 and NPF2.13 facilitate shoot-born GA loading into the phloem, we quantified GAs content in phloem exudates collected from leaf petioles. The double *npf2.12 npf2.13* loss-of-function mutant showed a striking reduction in GA_{12} content in the collected phloem exudates (**Fig. 5A**). Other GA metabolites (GA_{15}, GA_{24}, GA_9, GA_4, GA_{34}, and GA_{51}) were not significantly reduced (**Fig. 5A**). ABA levels showed a mild decrease, significant when compared to Col-0 using two-tailed t-tests but not significant when using Dunnett's multiple comparisons test ($p \leq 0.05$). The results imply that NPF2.12 and NPF2.13 regulate GA, and possibly ABA, loading into the shoot phloem. In agreement, quantification of active GA_4 content in the root, which is downstream to GA_{12} in the biosynthesis pathway, showed a significant reduction in the *npf12* and *npf13* single and double mutant lines (**Fig. 5B**). ABA content was also significantly lower in mutant roots compared to Col-0 (**Fig. 5B**).

To further test this hypothesis, we examined the expression pattern of the two transporters using reporter lines. In mature rosette, *NPF2.12* and *NPF2.13* were expressed in around the shoot apex and the main vascular vain (**Fig. 5C**). Cross-sections of *pNPF2.12:GUS* and *pNPF2.13:GUS* leaf petioles showed that both genes were expressed in the phloem companion cells (**Fig. 5C**). Next, we investigated whether these transporters are involved in long-distance GA movement from the shoot to the root. For this purpose, 16-day-old plants were grown on paclobutrazol, a GA biosynthesis inhibitor, for 4 days to deplete the plants of native GA, and GA_{12} was applied to a single leaf. We then quantified the DELLA protein REPRESSOR OF GA1-3 (RGA) abundance in the root. DELLA proteins act as repressors of the GA signal and are degraded in the presence of GA [54]. Time-course experiments in Col-0 plants showed a reduction in RGA accumulation in the root after GA_{12} treatment, indicating GA_{12} movement from the shoot to the root. On the other hand, in the *npf2.12 npf2.13* double mutant there was no RGA degradation (**Fig. 5D**), signifying a reduced GA accumulation in the root.

To understand how the NPF2.12 and NPF2.13 mediated long-distance GA transport influences root growth, we performed a series of micrografting between Col-0, *npf2.12 npf2.13* and GA-deficient *ga1-3* mutants and quantified root elongation rate. As expected, *ga1-3* self-grafts had a significantly lower root elongation rate than the Col-0 self-grafts. *npf2.12 npf2.13* self-grafts and Col-0 shoots grafted to *ga1-3* roots were indistinguishable from the Col-0 self-grafts (**Fig. 5E**). The fact that a wild-type shoot could rescue the *ga1-3* root elongation supports our hypothesis that GA can be transported from the shoot to the root to induce elongation. In comparison, *npf2.12 npf2.13* shoots grafted to *ga1-3* roots (*ga1-3/npf2.12 npf2.13*) showed a reduced root elongation compared to *ga1-3*/Col-0, indicating a partial requirement of NPF2.12 and NPF2.13 in long-distance GA transport (**Fig. 5E**). We hypothesize that once GA_{12} is translocated to the roots, it can be converted to the bioactive GA_4 by the GA20ox and GA3ox enzymes, which are expressed in the root [55]. Profiling the expression pattern of the *GA3ox* promoters, catalyzing the last step in bioactive GA_4 hormone synthesis, showed that expression of these enzymes is restricted to the stele as previously reported [55] (**Fig. 5F**). Together, these results imply that NPF2.12 and

NPF2.13 function in GA_{12} loading into the phloem for long-distance transport from the shoot to the root, with conversion to GA_4 taking place in the root stele.

Pericycle-specific vacuolar storage of GA and ABA at the phloem unloading zone facilitates endodermal suberin induction in the maturation zone.

To broaden our knowledge of GA and ABA distribution in the root and how it affects suberization, we created a mathematical model to simulate hormone distributions within the root cross-section, extending a modeling framework previously developed to study auxin transport [56] to incorporate a vacuole compartment within each cell. We present the model results for GA; the transport and resulting distribution for ABA would follow a similar pattern. Using a multicellular template segmented from a root-cross-sectional image (**Sup. Fig. 13**), we incorporated into the model experimentally observed distributions of root GA transporters: NPF3.1 on endodermal cell membranes [16,29], NPF2.12 on pericycle cell membranes (**Fig. 3I, 4A**), and NPF2.14 on the pericycle tonoplasts (**Fig. 1K, 2A**). The model simulated active GA transport via NPF3.1, NPF2.12, and NPF2.14, passive GA transport across both plasma membrane and tonoplast, GA synthesis and degradation, and GA diffusion within the apoplast with significantly reduced diffusion in the endodermal apoplast due to the presence of the Casparian strip.

To parameterize the model, permeabilities associated with each passive and active transport component were estimated using the oocyte data, and transport rates were then specified based on established pH and membrane potential values for plant cells [56–58] (**Sup. Table 4**). An important factor is the source of the hormone. *ABA2* and *AAO3*, which encode enzymes necessary for ABA biosynthesis, were previously shown to be expressed in the vasculature [59]. Bioactive GA_4 is also synthesized at high levels in the *Arabidopsis* stele [55] (**Fig. 5F**). Considering these data, together with the phloem unloading zone [41], the docking belt for the long-distance shoot-to-root transported hormones, led us to specify the stele as the source of active GA and ABA in the model. With these assumptions and parameterization, the model predicted the wild-type distribution of both cytoplasmic and vacuolar hormone concentrations for the 5-day-old plants used in the experiments (**Fig. 6A**). These predictions revealed high levels of both cytoplasmic and vacuolar GA in the endodermis, where suberization later occurs. Mutations in *npf3.1* and *npf2.12* were predicted to lead to a reduction in endodermal GA cytoplasmic concentrations (**Fig. 6A**), in agreement with the loss of endodermal GA-FI in these mutants (**Fig. 3G**) [16] and explaining their loss of suberization (**Fig. 4C**). Furthermore, while our experimental data suggested that NPF2.13 is not expressed in the root (**Fig. 4A**), the phloem sap and whole root GAs measurements suggest that NPF2.13 is an important contributor to the long-distance translocation of GA_{12} (**Fig. 6A**). The effects of the *npf2.13* mutation can be simulated by reducing the stele-specific synthesis rate. When the synthesis rate was reduced to represent mutation of *npf2.13*, the model predicted a reduction in GA concentrations throughout the root cross-section, again providing an explanation of the reduction in observed suberization (**Fig. 4C**). In contrast, simulation of the *npf2.14* mutation led to endodermal cytoplasmic GA concentrations that are higher than those in the wild-type, in agreement with the GA-FI accumulation at the elongation zone (**Fig. 1I**). Why *npf2.14* exhibits reduced suberization when endodermal accumulation

is higher remained unclear. However, predicted vacuolar concentrations in the *npf2.14* pericycle were much lower than in wild-type (**Fig. 6A**), leading us to hypothesize that NPF2.14 regulates GA levels both inside and outside of vacuoles in order to provide a GA source in the maturation zone, where GA is required for suberization. To test this hypothesis, we simulated the GA dynamics after reducing the synthesis rate to zero (mimicking cells leaving the phloem unloading zone) and found that the predicted endodermal cytoplasmic concentrations are maintained at higher levels with NPF2.14 present as cells mature (**Fig. 6B**). This suggests that the tonoplast pericycle-localized NPF2.14 ensures that GA concentrations are at levels necessary for mediation of suberization. Therefore, based on the model, we propose a pericycle-specific slow-release GA and ABA mechanism that explains how the two hormones are loaded into the pericycle vacuoles at the phloem unloading zone [41] and released from these vacuoles later on when the cells are mature (**Fig. 6B**). In this mechanism, GA and ABA unloaded from the phloem are transported into the pericycle and loaded into the vacuole to form a storage pool. When these cells reach the maturation zone, the GA and ABA that were stored in the pericycle vacuoles are transported by NPF3 into the endodermis to induce suberization.

In conclusion, the mathematical model confirmed that GA levels in the endodermis in wild-type roots were considerably higher than those in the *npf3.1*, *npf2.12*, and *npf2.13* roots. Furthermore, the tonoplast-localized NPF2.14 ensures that there is a vacuolar source of GA that enables the cross-section to maintain high endodermal GA levels after cells leave the phloem unloading zone [41]. The model predictions provide explanations for the suberization phenotypes observed in NPF mutants and emphasize that the pericycle is an NPF-mediated buffer-zone enabling cell-to-cell hormone movement from stele to endodermis.

Discussion

In this work, we identified *NPF2.14*, a previously uncharacterized transporter, as a dual-specificity GA and ABA vacuolar transporter. To the best of our knowledge, NPF2.14 is the first known sub-cellular GA/ABA transporter. We showed that *NPF2.14* is expressed in the pericycle to facilitate endodermal root suberization. Oocyte experiments showing that NPF2.14 exports GA from the cytosol, combined with NPF2.14's localization to the tonoplast, indicates that NPF2.14 transports GA and ABA from the cytosol into the vacuole.

The results presented here suggest that the pericycle serves as a buffer zone, regulating the transitions of hormones from the stele to the endodermis (Fig. 6C). The stele acts as the source of bioactive GA and ABA in the root [55,59]. Both hormones have been shown to accumulate and affect their respective response specifically in the endodermis [25,28,60,61]. In addition, it appears that the GA and ABA do not simply flow through the pericycle but rather are loaded into the vacuole by NPF2.14 to form a reservoir for later developmental stages. We propose that the high levels of GA and ABA present in the phloem unloading zone are taken into the pericycle by NPF2.12. Once in the pericycle cells, NPF2.14 facilitates their import into the vacuole for storage. We speculate that a slow-release mechanism feeds the differentiating cells with GA and ABA, thus allowing suberin formation in the mature root (Fig. 6C). Vacuoles have been

proposed to act as storage, modification, or degradation compartments for plant hormones [62]. It is possible that tonoplast-localized NPF2.14 mediates the hormonal homeostasis balance that is needed for the proper execution of the developmental plan in the neighboring cell file. At this point, it is not clear if GA and ABA are stored at their bioactive form in the vacuole.

Confocal imaging of the NLS-YFP lines indicated that both *NPF2.12* and *NPF2.14* are expressed in the pericycle, mainly in the phloem poles (Fig. 2A, 4A**)**. It is therefore possible that the hormone uptake is not carried uniformly throughout the pericycle ring, but rather amplified at the pericycle phloem poles cells. If so, do the two hormones retain polar distribution in the pericycle and in the subsequent endodermis layer? Or do the hormones have the ability to move within the two cell file rings? Future mathematical models and genetic work is required to address these questions.

The significantly reduced GA_{12} content in *npf2.12 npf2.13* double knockout phloem extracts implies that these transporters are required for GA_{12} loading into the phloem and translocation of GA_{12} from the shoot to the root. Thus, we hypothesize that NPF2.12 and NPF2.13, which are plasma membrane-localized importers expressed in the shoot phloem companion cells, are part of the long-sought mediators of long-distance GA shoot-to root translocation. Our results are in agreement with the previous finding that GA_{12} is the main form of GA that is transported long distances through the plant [12]. In addition, we showed that GA3ox1 and GA3ox2, which catalyze the final step of active GA production, are expressed in the root stele [55] (Fig. 5F). Thus, once GA_{12} docks at the root stele, it is converted by GA3ox1 and GA3ox2 into the bioactive GA_4 form, which is then delivered from the stele to the endodermis by NPF2.12 and NPF3.1 (Fig. 6C).

It is intriguing that NPF2.12 and NPF2.13 act as GA_{12} shoot-to-root transporters and also promote the delivery of the bioactive forms of GA and ABA to the endodermis. In both cases, a plasma membrane import activity is involved, but the substrate specificity differs. Since we showed that NPF2.12 and NPF2.13 are able to transport both intermediates of- and the bioactive forms of GA (Fig. 3B, **Sup. Figure 7**) and that GA_{12} is present at high levels in the shoot phloem (Fig. 5A), we speculate that GA_{12} is the primary substrate of the transporters. In the root stele, NPF2.12 recognizes bioactive ABA and GA_4, which are present in high concentrations due to being synthesized there [59].

The presented work showed for the first time that GA promotes suberization; ABA is known to participate in this process [49]. This explains the physiological importance of GA accumulation in the endodermis. At this stage, it is not clear whether GA promotes endodermis suberization directly by, for example, direct binding and activation of the suberin biosynthesis factor by DELLA or DELLA co-partners, or whether suberization is a secondary effect of maturation or signaling through the ABA components. GA and ABA are antagonistic hormones [63]; however, our data revealed that the two hormones can act non-antagonistically to promote root suberization. The results are in agreement with the growth defects displayed by biosynthesis mutants of these hormones, which result in small dark green plants [64–66].

Thus, it could be that the two hormones act synergistically to promote growth and other processes under normal or stress conditions.

Methods

Plant material and growth conditions

All *Arabidopsis thaliana* lines are in a Col-0 background. T-DNA insertion lines were supplied by the *Arabidopsis* Biological Resource Center. PCR genotyping for homozygous lines was performed using the primers listed in **Sup. Table 1.** To generate *npf2.12 npf2.13* double mutant, *npf2.12* (SALK_138987) was crossed to *npf2.13* (SALK_022429) to obtain an F1 population. F3 homozygous plant was selected by PCR genotyping.

Plants were sown on vertical plates containing 0.5 × Murashige-Skoog (MS) medium, 1% sucrose, and 0.8% agar, pH 5.7, stratified for 2 days at 4°C in the dark, then transferred to growth chambers (Percival CU41L5) at 21°C, 100 µE m^{-2} s^{-1} light intensity under long day light (16 h light/8 h dark). All plants in suberin quantification experiments were grown on 0.5 × MS medium, 1% sucrose, and 0.8% agar, pH 5.7 for 3 days and subsequently moved to 0.5 × MS medium without sucrose supplementation due to phenotype masking by the sucrose treatment. For low-nitrate experiments, plants were sown on MS with vitamins, nitrate free (Caisson labs MSP07-50LT), which was supplemented with 0.01 mM (Low nitrate) or 10 mM (High nitrate) KNO_3.

Hypocotyl cross sections

Sectioning and clearing were performed as describe in Ursache et al [44]. 3-Week-old hypocotyls were fixed in 4% PFA for an hour, rinsed twice in 1xPBS embedded in 5% agarose and sectioned to 150 µM slices using a Leica VT1000S vibratome. Slices were cleared using a ClearSee solution for 5 days. Following clearing sections were counterstained with 0.1% Calcofluor White in ClearSee solution for 30 min. Next, the seedlings were washed in ClearSee for 30 min with gentle shaking. For imaging, sections were mounted directly in ClearSee and imaged using a Zeiss LSM 780 inverted microscope.

Hormone application

Hormone was added to the agar medium at concentrations indicated in the figure legends. Seedlings were either germinated on media or moved after germination to treatment plates. GA-Fl (5 µM) was applied in liquid MS media for 16 h prior to imaging. For *ga1* experiments, both Col-0 and *ga1* seeds were imbibed in sterile water containing 5 µM GA_3 for 16 h to induce uniform germination. Following imbibition, seeds were washed three times in sterile water to wash away excess GA and were sown on MS plates.

Cloning of NPFs overexpression and reporter lines

NPF2.12 and *NPF2.14* coding sequences were synthesized by Bio Basic Inc., cloned into pENTR/D-TOPO (Invitrogen K2400), and subsequently cloned into the pH7YWG2 destination vectors using the LR Gateway reaction (Invitrogen 11791). *NPF2.12* and *NPF2.14* promoters were amplified with the primers listed in **Sup. Table 2** using a Phusion high-fidelity polymerase (New England Biolabs), cloned into pENTR/D-TOPO, and then cloned into pMDC7 vector for *NLS-YFP* reporters and pGWB3 vector for GUS reporters.

To generate *pNPF2.13:GUS* reporter, the promoter of *NPF2.13* (1.7-kb fragment) was PCR amplified from Col-0 genomic DNA with appropriate primers listed in **Sup. Table 2** and inserted into pDONR221 (Invitrogen) by Gateway cloning and recombined with pGWB633 [67].

Imaging and analysis

Seedlings were stained in 10 mg/L^{-1} propidium iodide (PI) for 5 min, rinsed, and mounted in water. Seedlings were imaged using a laser scanning confocal microscope (Zeiss LSM 780 inverted microscope), with argon laser set at 488 nm for fluorescein, 514 nm for YFP, and 561 nm for PI excitation. Emission filters used were 493-548 nm for fluorescein derivatives, 508-570 nm for YFP, and 583-718 nm for PI emission. Image analysis and signal quantification were done with the measurement function of ZEN lite software. The number of quantified biological repeats and sampling points is indicated for each graph in figure legends.

Root length characterization

For root length measurements, seedlings were imaged using Zeiss Stemi 2000-C stereo microscope and measured using ImageJ software (http://rsbweb.nih.gov/ij/index.html).

Histochemical GUS staining

Plants were immersed in 100 mM sodium phosphate buffer (pH 7.0) containing 0.1% Triton X-100, 1 mM 5-bromo-4-chloro-3-indolyl-β-D-glucuronic acid cyclohexylammonium salt (Sigma-Aldrich), 2 mM potassium ferricyanide, and 2 mM potassium ferrocyanide. Plants subject to vacuum treatment for 10 min and then incubated at 37 °C for 16 h. Tissues were cleared with 30%, 50%, and 70% ethanol for 30 min in each concentration and imaged using an AxioZoom 16, Zeiss binocular microscope.

For cross-sectioning of GUS-stained leaf petioles, after clearing in 70% ethanol, the samples were fixed in FAA solution (3.2% formaldehyde, 5% acetic acid, 50% ethanol) for 30 min and kept overnight at 4°C. The samples were then dehydrated in an ethanol gradient ranging from 50% to 96%, and incubated in 2% eosin overnight at 4° C. After several washes in 96% ethanol, the samples were progressively rehydrated in ethanol/HISTO-CLEAR II (Electron Microscopy Sciences) solution, incubated in 50% HISTO-CLEAR II 50% PARAPLAST PLUS (McCormick Scientific) at 60°C for 2 h, and embedded in 100% PARAPLAST PLUS. Paraffin-embedded samples were cross-sectioned with LEICA RM2155 microtome and imaged using a Leica Leitz Dmrb microscope.

Nile red suberin staining, imaging and quantification.

Nile red suberin staining was performed as described by Ursache et al. [44]. In short, 5-day-old seedlings were fixed in paraformaldehyde for 1 h under gentle agitation and washed twice in phosphate-buffered saline, pH 7.4. Plants were covered in filtered 0.05% Nile red (Acros Organics, 7385-67-3) solution dissolved in ClearSee for 16 h. Following staining, plants were washed three times in ClearSee for 30 min each wash. Next, plants were counterstained with 0.1% calcofluor white (Glentham Life Sciences, 4404-43-7) dissolved in ClearSee for cell wall imaging. After 30 min, plants were washed in ClearSee for 30 min. Plants were mounted directly in ClearSee on slides and imaged with a Zeiss LSM780 confocal microscope. Images were taken from the upper part of the root and under the root-hypocotyl junction with an argon laser set at 514 nm for Nile red excitation and 405 nm for calcofluor excitation. Emission filters used were 561-753 nm filter for Nile red and 410-511 nm filter for calcofluor emission. Fluorescence intensity was assessed using the Zen software from 5 endodermal cells per root.

Phylogenetic tree

Protein sequences for *Arabidopsis thaliana* NPF family members were retrieved from TAIR (https://www.arabidopsis.org). Phylogenetic relationships were defined using Phylogeny.fr (http://www.phylogeny.fr/) and visualized with FigTree software (http://tree.bio.ed.ac.uk/software/figtree/).

Transport assays in *Xenopus* oocytes

Coding sequences were cloned into the pNB1u vector, and complementary RNA (cRNA) was produced as described in Wulff et al. [34]. *Xenopus* oocyte assays were performed as described previously [34]. Defolliculated *Xenopus laevis* oocytes (stage V-VI) were purchased from Ecocyte Biosciences and were injected with 25 ng cRNA in 50.6 nl using a Drummond Nanoject II and incubated for 2-4 days at 16 °C in HEPES-based kulori (90 mM NaCl, 1 mM KCl, 1 mM $MgCl_2$, 1 mM $CaCl_2$, 5 mM HEPES, pH 7.4) before use. Oocytes were pre-incubated in MES-based kulori (90 mM NaCl, 1 mM KCl, 1 mM $MgCl_2$, 1 mM $CaCl_2$, 5 mM MES, pH 5) for 4 min and were then transferred to phytohormone-containing MES-based kulori for 60 min. After washing three times in 25 ml HEPES-based kulori followed by one wash in 25 ml deionized water, oocytes were homogenized in 50% methanol and stored for >30 min at -20 °C. Following centrifugation (25000 g for 10 min 4 °C), the supernatant was mixed with deionized water to a final methanol concentration of 20% and filtered through a 0.22-µm filter (MSGVN2250, Merck Millipore) before analytical LC-MS/MS as described below. For nitrate assays, sodium chloride in kulori was substituted for equimolar sodium nitrate in order not to affect the membrane potential.

Quantification of phytohormone content by LC-MS/MS

Compounds in the diluted oocyte extracts were directly analyzed by LC-MS/MS. The analysis was performed with modifications from the method described in Tal et al. [16]. In brief, chromatography was performed on an Advance UHPLC system (Bruker). Separation was achieved on a Phenomenex Kinetex

1.7u XB-C18 column (100 x 2.1 mm, 1.7 µm, 100 Å) with 0.05% v/v formic acid in water as mobile phase A and acetonitrile with 0.05% formic acid (v/v) as mobile phase B. The gradients used for elution of GAs were 0-0.5 min, 2% B; 0.5-1.3 min, 2-30% B; 1.3-2.2 min 30-100% B, 2.2-2.8 min 100% B; 2.8-2.9 min 100-2% B; and 2.9-4.0 min 2% B. The gradients used for elution of ABA were 0-0.5 min, 2% B; 0.5-1.2 min, 2-30% B; 1.2-2.0 min, 30-100% B; 2.0-2.5 min, 100%; 2.5-2.6 min, 100-2% B; and 2.6-4.0 min, 2% B. The mobile phase flow rate was 400 µl min^{-1}, and column temperature was maintained at 40 °C. The liquid chromatography was coupled to an EVOQ Elite triple quadrupole mass spectrometer (Bruker) equipped with an electrospray ion source operated in positive and negative ionization mode. Instrument parameters were optimized by infusion experiments with pure standards. For analysis of GAs, the ion spray voltage was maintained at +4000 V and -4000 V in positive and negative ionization mode, respectively, and the heated probe temperature was set to 200 °C with probe gas flow at 50 psi. For ABA, the ion spray voltage was maintained at -3300 V in negative ionization mode, and heated probe temperature was set to 120 °C with probe gas flow at 40 psi. Remaining settings were identical for all analytical methods with cone temperature set to 350 °C and cone gas to 20 psi. Nebulizing gas was set to 60 psi and collision gas to 1.6 mTorr. Nitrogen was used as probe and nebulizing gas, and argon as collision gas. Active exhaust was constantly on. Multiple reaction monitoring was used to monitor analyte parent ion to product ion transitions for all analytes. Multiple reaction monitoring transitions and collision energies were optimized by direct infusion experiments. Detailed values for mass transitions can be found in **Supplemental Table 3**. Both Q1 and Q3 quadrupoles were maintained at unit resolution. Bruker MS Workstation software (Version 8.2.1) was used for data acquisition and processing. Linearity in ionization efficiencies were verified by analyzing dilution series of standard mixtures. Sinigrin glucosinolate was used as internal standard for normalization but not for quantification. Quantification of all compounds was achieved by external standard curves diluted with the same matrix as the actual samples. All GAs were analyzed together in a single method. GA_{12} suffered from severe ion suppression when combined with the other GAs in the standard curve, thus quantification was not achieved for GA_{12}.

Root suberin monomer profiling by GC-MS

Suberin monomers were extracted from Col-0 and mutant roots according to the protocols previously described by [68,69]. A sample volume of 1 µL was injected in splitless mode on a GC-MS system (Agilent 7693A Liquid Auto injector, 8860 gas chromatograph, and 5977B mass spectrometer). GC was performed (HP-5MS UI column; 30 m length, 0.250 mm diameter, and 0.25 µm film thickness; Agilent J&W GC Columns) with injection temperature of 270°C, interface set to 250°C, and the ion source to 200°C. Helium was used as the carrier gas at a constant flow rate of 1.2 mL min^{-1}. The temperature program was 0.5 min isothermal at 70°C, followed by a 30°C min^{-1} oven temperature ramp to 210°C and a 5°C min^{-1} ramp to 330°C, then kept constant during 21 min. Mass spectra were recorded with an *m/z* 40 to 850 scanning range. Chromatograms and mass spectra were evaluated using the MSD ChemStation software (Agilent). Integrated peaks of mass fragments were normalized for sample dry weight and the respective C32 alkane internal standard signal. For identification, the corresponding mass spectra and retention time indices were compared with the NIST20 library as well as in-house spectral libraries.

Xenopus oocyte injection based efflux transport assays

For injection-based export assays, on the second day of gene expression, oocytes were injected with 23 nl 8.2 mM in 98 mM KCl, 1 mM $CaCl_2$, 10 mM HEPES, pH 7.4. T1 oocytes were left 10 min to heal and were then transport was evaluated as described above. T2 oocytes were left for approximately 20 h in HEPES-based kulori at 16° C, followed by transport analysis.

Quantification of nitrate from oocytes by HPLC

Nitrate concentration in the oocyte extracts was quantified using a Dionex ICS-2100 anion exchange chromatography system (Thermo Scientific). The separation was done on a Dionex IonPac AG11-HC analytical column coupled to the AS11-HC guard column (Thermo Scientific). The columns were connected to a Dionex AERS 500 anion suppressor (Thermo Scientific). The analyses were performed under the following conditions: sample injection volume 4.8 µl, column temperature 30 °C, flow rate of 0.38 ml/min, isocratic eluent gradient using 30 mM KOH solution in QH_2O, suppressor current of 29 mA, and runtime of 15 min. The nitrate detection was done at 220 nm using a Dionex UltiMate 3000 (Thermo Scientific). QH_2O water dilutions of Dionex Combined Seven Anion Standard (Thermo Scientific) were used to create a standard calibration curve. Accuracy and precision of the quantification was checked by including samples of potassium nitrate throughout the sequence.

pH measurements of oocyte lumen

The pH stabilization was performed as described previously [34]. pH-electrodes were pulled from borosilicate glass capillaries (KWIK-FIL TW F120-3 with filament) on a vertical puller (Narishige Scientific Instrument Lab), baked for 120 min at 220 °C and silanized for 60 min with dimethyldichlorosilane (Silanization Solution I, Sigma Aldrich). Electrodes were backfilled with a buffer containing 40 mM KH_2PO_4, 23 mM NaOH and 150 mM NaCl (pH 7.5). The electrode tip was filled with a proton-selective ionophore cocktail (hydrogen ionophore I cocktail A, Sigma-Aldrich) by dipping the tip into the cocktail. Oocytes, as described above, were placed in freshly made HEPES-based ekulori (2 mM $LaCl_3$, 90 mM NaCl, 1 mM KCl, 1 mM $MgCl_2$, 1 mM $CaCl_2$, 5 mM HEPES pH 7.4) for at least 30 min prior to three-electrode voltage clamp experiments. Before each oocyte a pH calibration curve was made for each oocyte using 100 mM KCl pH 5.5, 100 mM KCl pH 6.5 and 100 mM KCl pH 7.5. Oocytes were clamped at 0 mV and perfused with HEPES-based ekulori pH 7.4, followed by MES-based ekulori (2 mM $LaCl_3$, 90 mM NaCl, 1 mM KCl, 1 mM $MgCl_2$, 1 mM $CaCl_2$, 5 mM MES pH 5) and internal pH response was measured continuously as a function of external pH change.

Membrane potential measurements

Membrane potentials of oocytes were measured using the automated two-electrode voltage clamp system, Roboocyte2 (Multi channel systems), in ekulori (90 mM NaCl, 1 mM KCl, 1 mM $MgCl_2$, 1 mM $CaCl_2$, 5 mM MES, 2 mM $LaCl_3$, pH 5) with electrodes backfilled with 1 M KCl and 1.5 M potassium

acetate. All oocytes were measured using the same electrodes with a resistance of 280-350 kΩ. The experiment was terminated when the resistance of one of the electrodes shifted to approximately 600 kΩ.

Two-electrode voltage clamp electrophysiology

The electric signal elicited by GA treatment of oocytes was measured using the automated two-electrode voltage clamp system Roboocyte2 (Multi channel systems), in ekulori (90 mM NaCl, 1 mM KCl, 1 mM $MgCl_2$, 1 mM $CaCl_2$, 5 mM MES, 2 mM LaCl3 pH 4.5 or pH 5) with electrodes (resistance 280-1000 kΩ) backfilled with 1 M KCl and 1.5 M potassium acetate. Oocytes were clamped at – 60 mV, and IV curves were obtained before and after substrate addition. Substrate dependent currents were calculated by subtracting currents before addition of substrate from currents after addition of substrate.

Root hormone quantification

Hormone extraction and analysis was performed as described in Zhang et al., 2021. Standards (both labelled and non-labelled) were obtained from Olchemim Ltd. (Olomouc, Czech Republic) and National Research Council (NRC-CNRC, Canada). Standard grade solvents were used for sample preparation, Methanol, Acetic acid (LiChrosolv, Sigma-Aldrich, USA), Acetonitrile (J.T.Baker, Avantor, PA, USA), Formic acid (Honeywell Fluka, Thermo Fisher Scientific, MA, USA) and de-ionized water (Milli-Q, Synergy-UV millipore system, USA). Briefly, root tissue frozen in liquid nitrogen was grounded using motor and pestle. Around 200 mg of root sample was measured from ground powder and extracted with ice cold methanol/water/formic acid (15/4/1 v/v/v) added with deuterium labelled internal standards (IS). Similar concentrations of IS of abscisic acid and gibberellin (GA_4) were added into samples and calibration standards. The samples were purified using Oasis MCX SPE cartridges (Waters, USA) according to manufacturer's protocol. The samples were injected on Acquity UPLC BEH C18 column (1.7 µm, 2.1x100 mm, Waters; with gradients of 0.1% acetic acid in water or acetonitrile), connected to Acquity UPLC H class system (with Waters Acquity QSM, FNR sample manager and PDA) coupled with UPLC-ESI-MS/MS triple quadrupole mass spectrometer (Xevo TQ-S, Waters, equipped with ESI probe) for identification and quantification of hormones. The hormones were measured using MS detector, both in positive and negative mode, with two MRM transitions for each compound. External calibration curves were constructed with hormone standards added with IS, used for quantification, and calculated through Target Lynx (v4.1; Waters) software by comparing the ratios of MRM peak areas of analyte to that of internal standard.

Phloem extract and hormone quantification

Rosette leaves of 5-week-old Col-0 and *npf2-12 npf2-13* mutant plants (before bolting) were cut with a razor blade at the base of the petiole, and each leaf was dipped in a tube containing 80 µL of exudation buffer (50 mM potassium phosphate buffer, pH7.6, 10 mM EDTA). Exudation was carried out for 3h in dark in high humidity to limit transpiration. Exudation of 75 leaves was regrouped and concentrated under vacuum centrifugation. Hormone contents in phloem exudates were determined by UPLC system-MS/MS (Waters Quattro Premier XE). Concentrated residue of phloem sap was resuspended with 80%

methanol-1% acetic acid including 17-$^{2}H_2$-labeled GA internal standards (Olchemim), mixed and passed through an Oasis HLB column. The dried eluate was dissolved in 5% acetonitrile-1% acetic acid, and the GAs were separated by UPHL chromatography (Accucore RP-MS column 2.6 µm, 100 x 2.1 mm; ThermoFisher Scientific) with a 5 to 50% acetonitrile gradient containing 0.05% acetic acid, at 400 µL/min over 22 min. The concentrations of GAs in the extracts were analyzed with a Q-Exactive mass spectrometer (Orbitrap detector; ThermoFisher Scientific) by targeted SIM using embedded calibration curves and the Xcalibur 2.2 SP1 build 48 and TraceFinder programs.

Grafting assays.

Grafting was performed without collars on water imbibed 0.45 µM MCE membrane (Millipore) between hypocotyls of rootstocks and scions of 6-day-old seedlings grown on 1x MS agar plate. Grafted seedlings were then kept vertically to recover, for 5 days under constant humidity. Successful grafts were transferred onto ½x MS agar plates and grown under a 16h photoperiod at 22°C. Root growth was measured every day for 4 days.

DELLA degradation assays.

12-day-old seedlings were transferred to 1x MS agar modified medium without nitrogen (bioWORLD plant media) supplemented with 0.5 mM KNO_3 and 1 µM paclobutrazol (Sigma). 4 days after transfer, a drop of GA_{12} (5 µl at 1 µM) was placed on one of the first two leaved formed. Roots were collected 6, 12 and 24h after adding GA_{12}. Total proteins were extracted in 2x SDS-PAGE sample buffer and separated on 10% SDS-PAGE gel. After transfer onto membrane, immunoblots were performed using a 2000-fold dilution anti-RGA (Agrisera) and a 10000-fold dilution of peroxidase-conjugated goat anti-rabbit (Thermo Fisher Scientific). Signals were detected with Fusion FX (Vilber) using Immobilon Forte Western HRP Substrate (Millipore). The blot was subsequently stained with Coomassie blue. Quantification of the signals was determined using ImageJ package.

Mathematical model.

Root templates were segmented from an experimental image using the CellSeT image analysis tool [70] (**Sup. Fig. 13**). We used CellSeT to manually assign a cell type to each cell and then read the geometrical and cell-type data into a tissue database (based on the OpenAlea tissue structure [71]), extending the data structure to incorporate vacuolar compartments within each cell. The geometrical, topological and transporter-distribution data were used to form a system of ordinary differential equations (ODEs) to describe the GA transport, synthesis and degradation within the multicellular root cross-section. Parameters associated with the passive and transporter-mediated transport components were estimated using the oocyte data (**Fig. 1A, Fig. 3B**) and the remaining parameter values were obtained from the literature (**Sup. Table 4**). These ODEs were simulated using the solve_ivp package in python 3.6.5. Full details of the model equations and assumptions are provided as Supplementary text.

Declarations

Acknowledgments

We thank Daria Binenbaum for the illustrations and Peter Hedden (Rothamsted Research) for sharing *pGA3ox1-4:GUS* seeds. Funding: This work was supported by grants from the Israel Science Foundation (2378/19 and 3419/20 to E.S.), the Human Frontier Science Program (HFSP—RGY0075/2015 and HFSP—LIY000540/2020 to E.S., H.H.N.-E. and L.R.B.), Danmarks Grundforskningsfond (DNRF99 to H.H.N.-E.), the European Research Council (757683-RobustHormoneTrans to E.S.), the Constantiner Travel Fellowship (to J.B.), the Centre National de la Recherche Scientifique (to L.S-A. J-M.D. and P.A.), the French Ministry of Research and Higher Education studentship (to L.C.).

Author contributions

J.B. performed the research and wrote the manuscript. N.W. performed the oocyte transporter assays. L.C., L.S-A., J-M.D. and P.A carried out long-distance transport assays. K.K. performed the mathematical modelling. I.T. assisted in cloning overexpression and reporter lines. H.V. and A.A. quantified root GA and ABA content. M.A. helped with genotyping T-DNA mutant lines. Y.Z. helped with *npf* mutant identification. D.R. and L.R. assisted in cross sectioning and staining. E.C. quantified hormone content in the phloem sap. E.M. and H.C. performed suberin monomer quantifications. S.L. and R.W. synthesized fluorescently tagged hormones. V.N. and C.C. helped with nitrate and hormones quantification in oocyte assays, respectively. L.B., P.A., H.H.N.-E. and ES designed and supervised the work and edited the manuscript. All authors discussed the results and commented on the manuscript.

Competing interests: The authors declare that they have no competing interests.

Data and materials availability: All the data supporting the findings of this study are available within the article and the Supplementary Materials.

References

1. Hedden, P. & Sponsel, V. A Century of Gibberellin Research. J. Plant Growth Regul. **34**, 740–760 (2015).
2. Eriksson, S., Böhlenius, H., Moritz, T. & Nilsson, O. GA4 Is the Active Gibberellin in the Regulation of LEAFY Transcription and Arabidopsis Floral Initiation. Plant Cell **18**, 2172–2181 (2006).
3. Proebsting, W. M., Hedden, P., Lewis, M. J., Croker, S. J. & Proebsting, L. N. Gibberellin Concentration and Transport in Genetic Lines of Pea Effects of Grafting. Plant Physiol. **100**, 1354–1360 (1992).
4. Björklund, S., Antti, H., Uddestrand, I., Moritz, T. & Sundberg, B. Cross-talk between gibberellin and auxin in development of Populus wood: gibberellin stimulates polar auxin transport and has a common transcriptome with auxin. Plant J. **52**, 499–511 (2007).

5. Dayan, J. *et al.* Leaf-Induced Gibberellin Signaling Is Essential for Internode Elongation, Cambial Activity, and Fiber Differentiation in Tobacco Stems. Plant Cell **24**, 66–79 (2012).
6. Chin, T. Y. & Lockhart, J. A. TRANSLOCATION OF APPLIED GIBBERELLIN IN BEAN SEEDLINGS. Am. J. Bot. **52**, 828–833 (1965).
7. ZWEIG, G., YAMAGUCHI, S. & MASON, G. W. Translocation of C 14 -Gibberellin in Red Kidney Bean, Normal Corn, and Dwarf Corn. 122–134 (1961).
8. Hoad, G. V. & Bowen, M. R. Evidence for gibberellin-like substances in phloem exudate of higher plants. Planta **82**, 22–32 (1968).
9. Hu, J. *et al.* Potential Sites of Bioactive Gibberellin Production during Reproductive Growth in Arabidopsis. Plant Cell **20**, 320–336 (2008).
10. Weiss, D. & Halevy, A. H. Stamens and gibberellin in the regulation of corolla pigmentation and growth in Petunia hybrida. Planta **179**, 89–96 (1989).
11. Hedden, P. & Thomas, S. G. Gibberellin biosynthesis and its regulation. Biochem. J. **444**, 11–25 (2012).
12. Regnault, T. *et al.* The gibberellin precursor GA12 acts as a long-distance growth signal in Arabidopsis. Nat. Plants **1**, 1–6 (2015).
13. Camut, L. *et al.* Root-derived GA12 contributes to temperature-induced shoot growth in Arabidopsis. Nat. Plants **5**, 1216–1221 (2019).
14. Chiba, Y. *et al.* Identification of Arabidopsis thaliana NRT1/PTR FAMILY (NPF) proteins capable of transporting plant hormones. J. Plant Res. **128**, 679–686 (2015).
15. Kanno, Y. *et al.* AtSWEET13 and AtSWEET14 regulate gibberellin-mediated physiological processes. Nat. Commun. **7**, 1–11 (2016).
16. Tal, I. *et al.* The Arabidopsis NPF3 protein is a GA transporter. Nat. Commun. **7**, 1–11 (2016).
17. Saito, H. *et al.* The jasmonate-responsive GTR1 transporter is required for gibberellin-mediated stamen development in Arabidopsis. Nat. Commun. **6**, 1–11 (2015).
18. Corratgé-Faillie, C. & Lacombe, B. Substrate (un)specificity of Arabidopsis NRT1/PTR FAMILY (NPF) proteins. J. Exp. Bot. **68**, 3107–3113 (2017).
19. Nour-Eldin, H. H. *et al.* NRT/PTR transporters are essential for translocation of glucosinolate defence compounds to seeds. Nat. **488**, 531–534 (2012).
20. Kramer, E. M. How Far Can a Molecule of Weak Acid Travel in the Apoplast or Xylem? Plant Physiol. **141**, 1233–1236 (2006).
21. Binenbaum, J., Weinstain, R. & Shani, E. Gibberellin Localization and Transport in Plants. Trends Plant Sci. **23**, 410–421 (2018).
22. Zhu, J. K. Abiotic Stress Signaling and Responses in Plants. Cell **167**, 313–324 (2016).
23. Cutler, S. R., Rodriguez, P. L., Finkelstein, R. R. & Abrams, S. R. Abscisic Acid: Emergence of a Core Signaling Network. **61**, 651–679 (2010).

24. Liu, X. & Hou, X. Antagonistic regulation of ABA and GA in metabolism and signaling pathways. Front. Plant Sci. **9**, 251 (2018).
25. Ubeda-Tomás, S. *et al.* Root growth in Arabidopsis requires gibberellin/DELLA signalling in the endodermis. Nat. Cell Biol. **10**, 625–628 (2008).
26. Ubeda-Tomás, S. *et al.* Gibberellin Signaling in the Endodermis Controls Arabidopsis Root Meristem Size. Curr. Biol. **19**, 1194–1199 (2009).
27. Duan, L. *et al.* Endodermal ABA Signaling Promotes Lateral Root Quiescence during Salt Stress in Arabidopsis Seedlings. Plant Cell **25**, 324–341 (2013).
28. Shani, E. *et al.* Gibberellins accumulate in the elongating endodermal cells of Arabidopsis root. *Proc. Natl. Acad. Sci.* **110**, 4834–4839 (2013).
29. David, L. C. *et al.* N availability modulates the role of NPF3.1, a gibberellin transporter, in GA-mediated phenotypes in Arabidopsis. Planta **244**, 1315–1328 (2016).
30. Andersen, T. G., Barberon, M. & Geldner, N. Suberization — the second life of an endodermal cell. Curr. Opin. Plant Biol. **28**, 9–15 (2015).
31. Shukla, V. & Barberon, M. Building and breaking of a barrier: Suberin plasticity and function in the endodermis. Curr. Opin. Plant Biol. **64**, 102153 (2021).
32. Barberon, M. The endodermis as a checkpoint for nutrients. New Phytol. **213**, 1604–1610 (2017).
33. Zhang, Y. *et al.* ABA homeostasis and long-distance translocation are redundantly regulated by ABCG ABA importers. Sci. Adv. **7**, (2021).
34. Wulff, N. *et al.* An Optimized Screen Reduces the Number of GA Transporters and Provides Insights Into Nitrate Transporter 1/Peptide Transporter Family Substrate Determinants. Front. Plant Sci. **0**, 1106 (2019).
35. Jørgensen, M. E. *et al.* A Functional EXXEK Motif is Essential for Proton Coupling and Active Glucosinolate Transport by NPF2.11. Plant Cell Physiol. **56**, 2340–2350 (2015).
36. Solcan, N. *et al.* Alternating access mechanism in the POT family of oligopeptide transporters. EMBO J. **31**, 3411–3421 (2012).
37. Tsay, Y. F., Schroeder, J. I., Feldmann, K. A. & Crawford, N. M. The herbicide sensitivity gene CHL1 of arabidopsis encodes a nitrate-inducible nitrate transporter. Cell **72**, 705–713 (1993).
38. Campilho, A., Nieminen, K. & Ragni, L. The development of the periderm: the final frontier between a plant and its environment. Curr. Opin. Plant Biol. **53**, 10–14 (2020).
39. Beeckman, T., Burssens, S. & Inzé, D. The peri-cell-cycle in Arabidopsis. J. Exp. Bot. **52**, 403–411 (2001).
40. Takano, J. *et al.* Arabidopsis boron transporter for xylem loading. Nat. 2002 4206913 **420**, 337–340 (2002).
41. Ross-Elliott, T. J. *et al.* Phloem unloading in arabidopsis roots is convective and regulated by the phloempole pericycle. Elife **6**, (2017).

42. Wunderling, A. *et al.* A molecular framework to study periderm formation in Arabidopsis. New Phytol. **219**, 216–229 (2018).
43. Barberon, M. *et al.* Adaptation of Root Function by Nutrient-Induced Plasticity of Endodermal Differentiation. Cell **164**, 447–459 (2016).
44. Ursache, R., Andersen, T. G., Marhavý, P. & Geldner, N. A protocol for combining fluorescent proteins with histological stains for diverse cell wall components. Plant J. **93**, 399–412 (2018).
45. Lux, A., Morita, S., Abe, J. & Ito, K. An Improved Method for Clearing and Staining Free-hand Sections and Whole-mount Samples. Ann. Bot. **96**, 989–996 (2005).
46. Kreszies, T., Schreiber, L. & Ranathunge, K. Suberized transport barriers in Arabidopsis, barley and rice roots: From the model plant to crop species. J. Plant Physiol. **227**, 75–83 (2018).
47. Woolfson, K. N., Esfandiari, M. & Bernards, M. A. Suberin Biosynthesis, Assembly, and Regulation. Plants. **11**, 555 (2022).
48. Aloni, R. Vascular Differentiation and Plant Hormones. Vasc. Differ. Plant Horm. (2021).
49. Wang, C. *et al.* Developmental programs interact with abscisic acid to coordinate root suberization in Arabidopsis. Plant J. **104**, 241–251 (2020).
50. Sunai', T.-P. & Kamiya, Y. The Arabidopsis GA1 locus encodes the cyclase ent-kaurene synthetase A of gibberellin biosynthesis. Plant Cell **6**, 1509–1518 (1994).
51. Lin, Q. *et al.* The SnRK2-APC/CTE regulatory module mediates the antagonistic action of gibberellic acid and abscisic acid pathways. Nat. Commun. **6**, 1–10 (2015).
52. Almagro, A., Lin, S. H. & Tsay, Y. F. Characterization of the Arabidopsis Nitrate Transporter NRT1.6 Reveals a Role of Nitrate in Early Embryo Development. Plant Cell **20**, 3289–3299 (2009).
53. Fan, S. C., Lin, C. S., Hsu, P. K., Lin, S. H. & Tsay, Y. F. The Arabidopsis Nitrate Transporter NRT1.7, Expressed in Phloem, Is Responsible for Source-to-Sink Remobilization of Nitrate. Plant Cell **21**, 2750–2761 (2009).
54. Sun, T. P. The Molecular Mechanism and Evolution of the GA–GID1–DELLA Signaling Module in Plants. Curr. Biol. **21**, R338–R345 (2011).
55. Barker, R. *et al.* Mapping sites of gibberellin biosynthesis in the Arabidopsis root tip. New Phytol. **229**, 1521–1534 (2021).
56. Band, L. R. *et al.* Systems Analysis of Auxin Transport in the Arabidopsis Root Apex. Plant Cell **26**, 862–875 (2014).
57. Mathieu, Y. *et al.* Regulation of Vacuolar pH of Plant CellsI. Isolation and Properties of Vacuoles Suitable for 31P NMR Studies. Plant Physiol. **89**, 19–26 (1989).
58. Hedrich, R., Mueller, T. D., Becker, D. & Marten, I. Structure and Function of TPC1 Vacuole SV Channel Gains Shape. Mol. Plant **11**, 764–775 (2018).
59. Kuromori, T., Sugimoto, E. & Shinozaki, K. Intertissue Signal Transfer of Abscisic Acid from Vascular Cells to Guard Cells. Plant Physiol. **164**, 1587–1592 (2014).

60. De Diego, N. *et al.* Immunolocalization of IAA and ABA in roots and needles of radiata pine (Pinus radiata) during drought and rewatering. Tree Physiol. **33**, 537–549 (2013).
61. Ondzighi-Assoume, C. A., Chakraborty, S. & Harris, J. M. Environmental Nitrate Stimulates Abscisic Acid Accumulation in Arabidopsis Root Tips by Releasing It from Inactive Stores. Plant Cell **28**, 729–745 (2016).
62. Martinoia, E., Meyer, S., De Angeli, A. & Nagy, R. Vacuolar transporters in their physiological context. Annu. Rev. Plant Biol. **63**, 183–213 (2012).
63. Shu, K., Zhou, W., Chen, F., Luo, X. & Yang, W. Abscisic acid and gibberellins antagonistically mediate plant development and abiotic stress responses. Front. Plant Sci. **9**, 416 (2018).
64. Peng, J. & Harberd, N. P. Gibberellin Deficiency and Response Mutations Suppress the Stem Elongation Phenotype of Phytochrome-Deficient Mutants of Arabidopsis'. Plant Physiol 113 (1997).
65. González-Guzmán, M. *et al.* The Short-Chain Alcohol Dehydrogenase ABA2 Catalyzes the Conversion of Xanthoxin to Abscisic Aldehyde. Plant Cell **14**, 1833–1846 (2002).
66. Merilo, E. *et al.* Stomatal VPD Response: There Is More to the Story Than ABA. Plant Physiol. **176**, 851 (2018).
67. Nakamura, S. *et al.* Gateway Binary Vectors with the Bialaphos Resistance Gene, bar, as a Selection Marker for Plant Transformation. OUP **74**, 1315–1319 (2014).
68. Cohen, H. *et al.* A Multilevel Study of Melon Fruit Reticulation Provides Insight into Skin Ligno-Suberization Hallmarks. Plant Physiol. **179**, 1486–1501 (2019).
69. Cohen, H., Fedyuk, V., Wang, C., Wu, S. & Aharoni, A. SUBERMAN regulates developmental suberization of the Arabidopsis root endodermis. Plant J. **102**, 431–447 (2020).
70. Pound, M. P., French, A. P., Wells, D. M., Bennett, M. J. & Pridmorea, T. P. CellSeT: Novel Software to Extract and Analyze Structured Networks of Plant Cells from Confocal Images. Plant Cell **24**, 1353 (2012).
71. Pradal, C. *et al.* OpenAlea: a visual programming and component-based software platform for plant modelling. Funct. Plant Biol. **35**, 751–760 (2008).

Figures

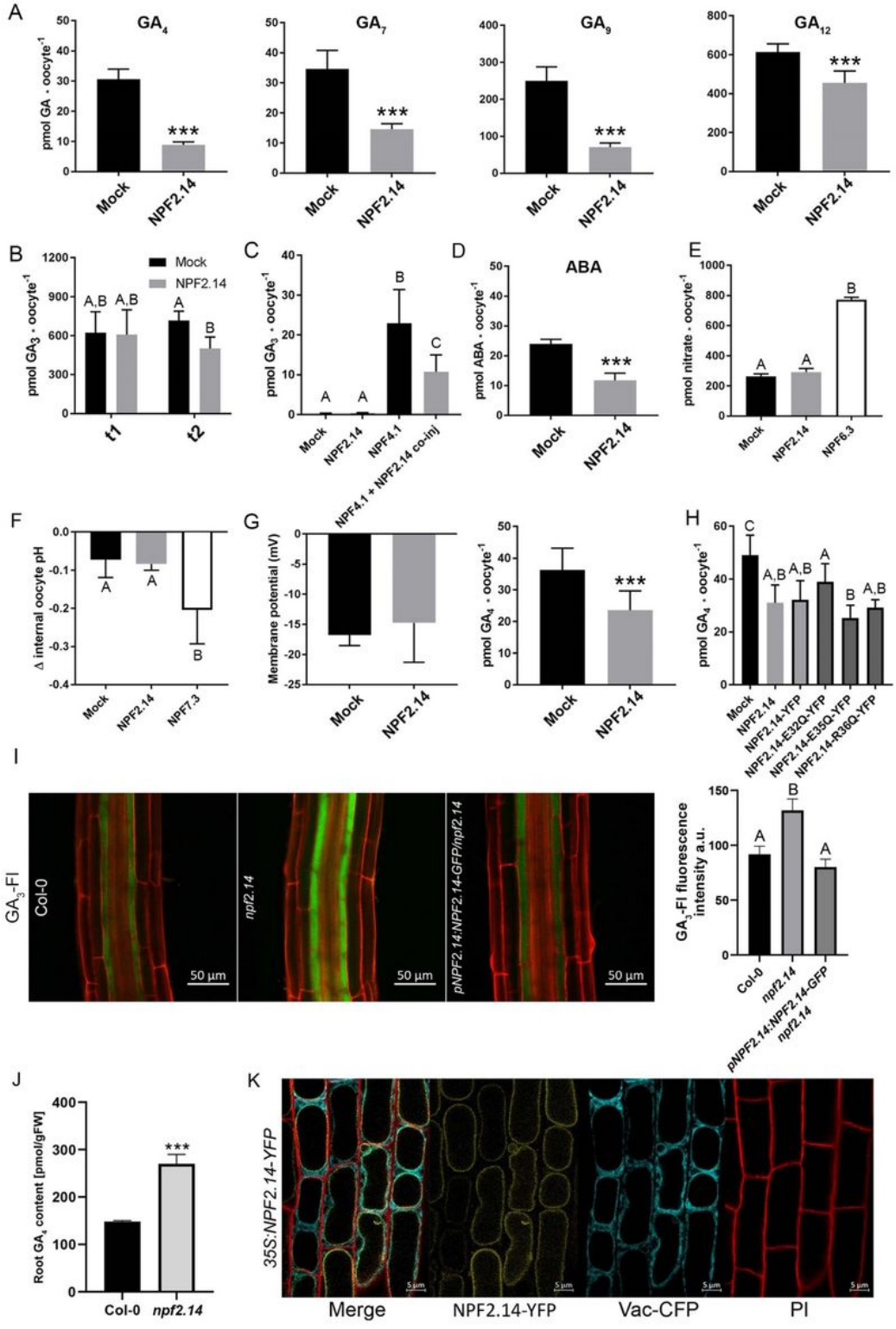

Figure 1

NPF2.14 is a vacuolar GA and ABA transporter. (**A**) GA accumulation in NPF2.14-expressing and control oocytes exposed to the indicated GAs at 50 µM concentration for 60 min at room temperature at pH 5 for GA_4 and GA_7 and at pH 6 for GA_9 and GA_{12} (n = 5 for GA_4, GA_7, and GA_9 and n = 6 for GA_{12}). Statistical significance was evaluated by two-tailed t-tests ($p \leq 0.05$). (**B**) GA accumulation at 20 h after direct injection of 23 nl of 8.2 mM membrane impermeable GA_3 at pH 7.4 at 16° C (t1) and after 60 min at room

temperature at pH 5 (t2) (n = 6). Statistical significance was determined by Holm Sidak two-way ANOVA ($p \leq 0.05$). (**C**) GA accumulation in control oocytes or oocytes that express NPF2.14, NPF4.1, or both proteins exposed to 50 µM GA_3 at pH 5 for 60 min at room temperature and analyzed by LC-MS/MS (n = 7). Statistical significance was assessed using a Holm Sidak one-way ANOVA ($p = 0.05$). (**D**) ABA accumulation in oocytes exposed to 50 µM ABA at pH 5 for 60 min at room temperature (n = 5). Statistical significance was determined by two-tailed t-test ($p = 0.05$). (**E**) Nitrate accumulation in oocytes exposed to 5 mM nitrate at pH 5 at room temperature for 60 min (three replicates of 5 oocytes analyzed by analytical anion chromatography). Statistical significance was assessed using a Holm Sidak one-way ANOVA ($p = 0.05$). (**F**) Internal oocyte pH measured using three-electrode voltage clamp electrophysiology of control oocytes and NPF2.14- and NPF7.3-expressing oocytes. Oocytes were perfused at pH 7.4 for 5 min followed by perfusion at pH 5 for 5 min (n = 4-6 single oocytes). Statistical significance was assessed using Holm Sidak one-way ANOVA ($p = 0.05$). (**G**) Membrane potentials of control oocytes (n = 12) and NPF2.14-expressing oocytes (n = 19) measured at pH 5 using two-electrode voltage clamp electrophysiology. Oocytes with measured membrane potential were exposed to 50 µM GA_4 at pH 5 (n = 7 single oocytes) for 60 min at room temperature and analyzed by LC-MS/MS. Statistical significance was assessed using two-tailed t-tests (*** $p < 0.001$). (**H**) GA accumulation in control oocytes or oocytes that express NPF2.14 with wild-type or mutant ExxE[K/R] motifs exposed to 50 µM GA_4 at pH 5 for 60 min at room temperature and analyzed by LC-MS/MS (n = 7). Statistical significance was assessed using a Holm Sidak one-way ANOVA ($p = 0.05$). (**I**) Left: Representative images of 6-day-old *npf2.14* mutant and *npf2.14* complementation lines. Roots were treated with 5 µM GA_3-Fl (green); propidium iodide (red). Right: GA_3-Fl fluorescence intensity in the endodermis, mean ± S.E (5 endodermal cells sampled from a minimum of 7 biological repeats, n > 35). (**J**) GA_4 content in 10-day-old roots of control and *npf2.14*-mutant plants measured using LC-MS. n = 5. Significance was evaluated using a Student's t-test (*** $p \leq 0.0001$). (**K**) Representative confocal image of 6-day-old root epidermis *35S:NPF2.14-YFP* cells stained with propidium iodide (red) and tonoplast marker Vac-CFP (cyan) (Nelson et al., 2007).

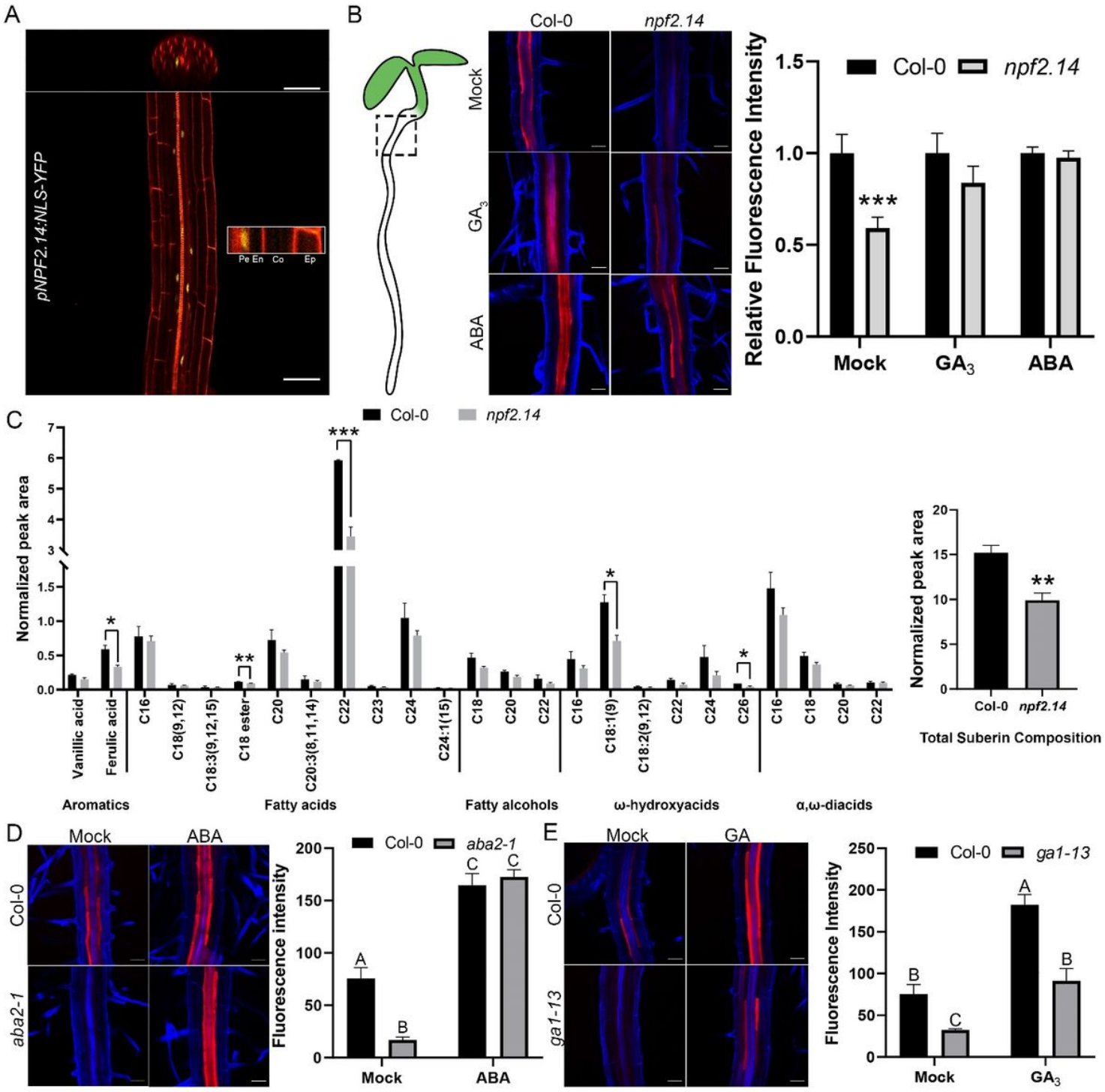

Figure 2

***NPF2.14* expression in the differentiated pericycle is required for endodermal root suberization.** (**A**) Confocal image of 6-day-old *pNPF2.14:NLS-YFP* roots stained with propidium iodide (red) and imaged for YFP (yellow). Inset is magnification of cells with *pNPF2.14:NLS-YFP* signal. Pe – Pericycle, En - Endodermis, Co – Cortex, Ep – Epidermis. (**B**) Left: Images of 5-day-old Col-0 and *npf2.14* mutant roots supplemented with mock solution, 5 µM GA_3, or 1 µM ABA and stained with Nile red (red) and calcofluor (blue). Right: Quantification of Nile red fluorescence intensity was normalized to Col-0 for each treatment.

Illustration indicates imaged area Fluorescent intensity was quantified from a minimum of 10 roots per treatment, 5 endodermal cells per root, n > 50. Statistical significance was assessed using a Dunnett's test (*** $p < 0.001$). (**C**) Root suberin profile measured by gas chromatography-mass spectrometry. The *y*-axis represents relative peak areas following normalization to a C_{32}-alkane internal standard. Right graph indicates for total suberin composition. Data in bars represent the means ± SE of three biological replicates. * indicates statistically significant differences compared with Col-0 at $p \leq 0.05$, ** $p \leq 0.01$ and *** $p \leq 0.001$ by Student's t-test.

(**D**) Left: Images of 5-day-old Col-0 and *aba2-1* roots from plants grown on mock MS or MS with 1 µM ABA. Roots were stained with Nile red (red) and calcofluor (blue). Right: Fluorescent intensity was quantified from a minimum of 10 roots per treatment, 5 endodermal cells per root, n > 50. Significance was determined using Tukey's ad-hoc statistical test (treatments marked with different letters are significantly different). (**E**) Left: Images of 5-day-old Col-0 and *ga1-13* mutant roots from plants grown on mock MS or MS with 5 µM GA. Roots were stained with Nile red (red) and calcofluor (blue). Right: Fluorescent intensity was quantified from a minimum of 8 roots per treatment, 5 endodermal cells per root, n > 40. Significance was determined using Tukey's ad-hoc statistical test (treatments marked with different letters are significantly different).

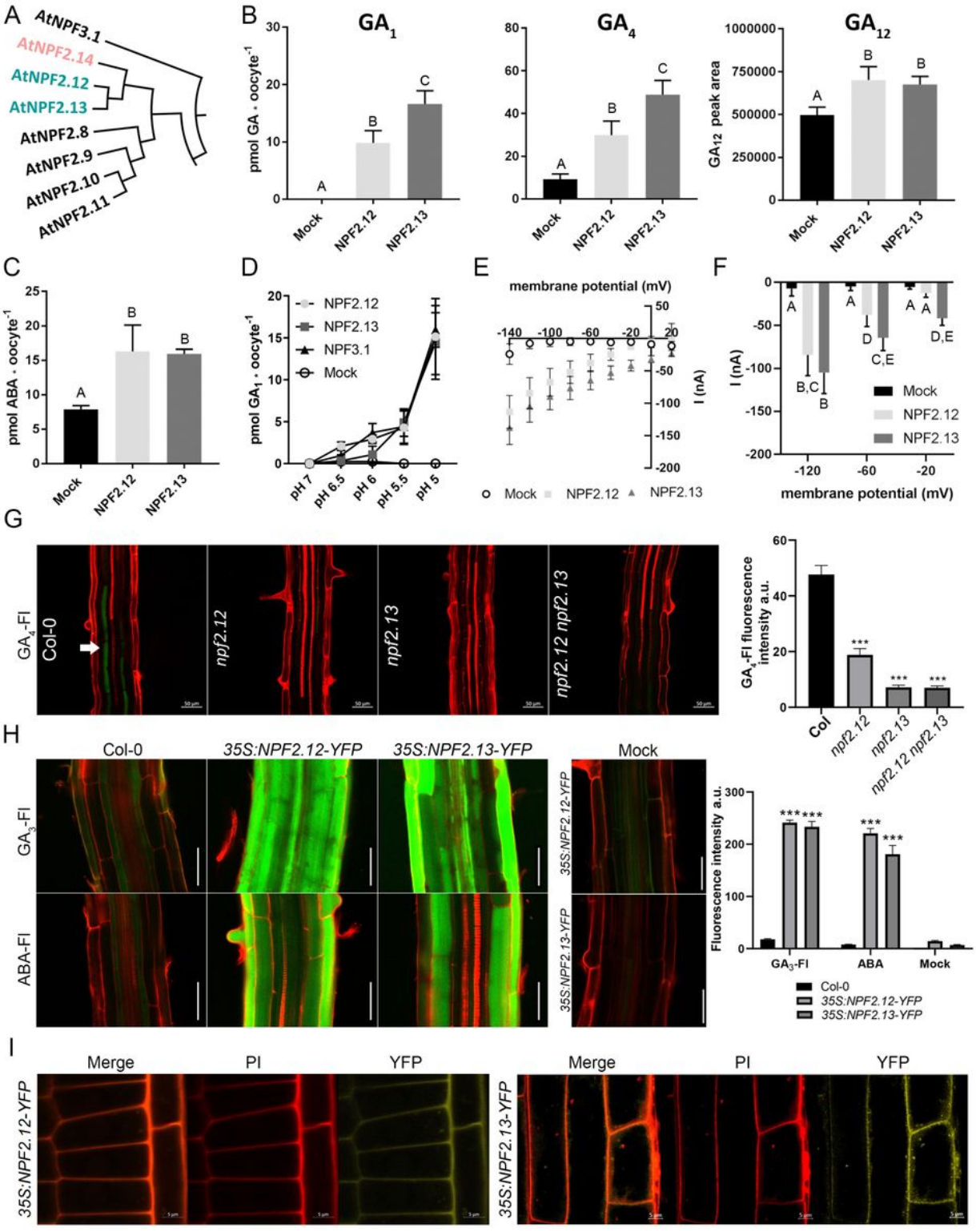

Figure 3

NPF2.12 and NPF2.13 are plasma membrane-localized GA and ABA importers that facilitate endodermal hormone accumulation. (**A**) Phylogenetic clade of *NPF2.12, NPF2.13, NPF2.14*, and their close paralogs. (**B and C**) Hormone uptake in control and NPF2.12- and NPF2.13-expressing *Xenopus* oocytes. **B)** Oocytes were exposed to 50 μM GA_1 at pH 5 (n = 5 single oocytes), 50 μM GA_4 at pH 5.5 (n = 5), or 50 μM GA_{12} at pH 6 (n = 5). (**C**) Oocytes were exposed to 50 μM ABA at pH 5 (n = 5). Hormone uptake was

analyzed by LC-MS/MS. Statistical significance was assessed using Holm Sidak one-way ANOVA (p = 0.05). (**D**) Oocytes were exposed to 50 μM GA_1 at pH ranging from 5 to 7 (n = 5). (**E and F**) Control oocytes (n = 10), oocytes expressing NPF2.12 (n = 9), and oocytes expressing NPF2.13 (n = 8) were exposed to 500 μM GA_3 at pH 5, and currents were measured using two-electrode voltage clamp electrophysiology over a range of membrane potentials from +20 to -140 mV. Statistical significance was assessed using Holm Sidak two-way ANOVA (p = 0.01). (**G**) Left: Representative images of roots of 6-day-old Col-0 and single and double *npf2.12* and *npf2.13* knockout plants treated with 5 μM GA_4-Fl (green) overnight. Red indicates propidium iodide. The white arrow indicates GA_4-Fl signal. Right: Quantification of GA_4-Fl fluorescence intensity in the endodermis, mean ± S.E. (5 endodermal cells were sampled from 3 biological repeats, n = 15). Significance was determined by Dunnett's multiple comparisons test (*** $p \leq$ 0.0001). (**H**) Left: Representative images of roots of 6-day-old *35S:NPF2.12-YFP* and *35S:NPF2.13-YFP* plants treated with 5 μM GA_3-Fl and ABA-Fl for 2 hours. Red indicates propidium iodide, green indicates GA_3-Fl or ABA-Fl. Right: GA_3-Fl and ABA-Fl fluorescence intensity was quantified in the epidermal cells, mean ± S.E. (5 epidermal cells sampled from at least 4 biological repeats, n > 20). *35S:NPF2.12-YFP* and *35S:NPF2.13-YFP* mock do not show fluorescence under these confocal gain settings. (**I**) Confocal imaging of 6-day old root cells expressing *35S:NPF2.12-YFP* and *35S:NPF2.13-YFP*. Red is PI, yellow is YFP.

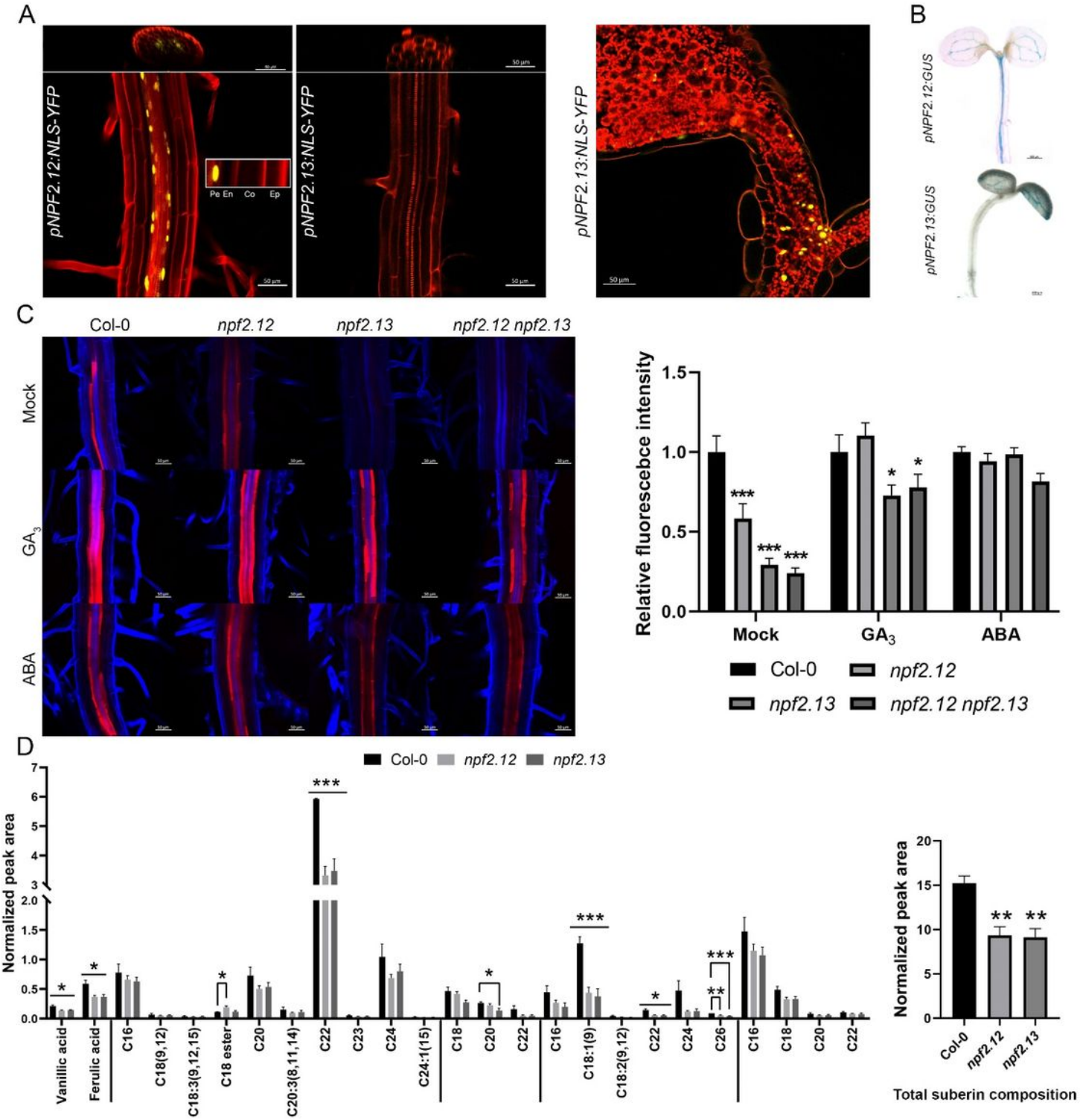

Figure 4

***NPF2.12* and *NPF2.13* regulate root endodermis suberization.** (**A**) Confocal imaging of 6-day-old *pNPF2.12:NLS-YFP* and *pNPF2.13:NLS-YFP* seedlings. Inset is magnification of cells with *pNPF2.12:NLS-YFP* signal. Pe – Pericycle, En - Endodermis, Co – Cortex, Ep – Epidermis. Red indicates either calcofluor (Left) or propidium iodide (Right), yellow indicates YFP. (**B**) GUS staining of 6-day-old seedlings expressing *pNPF2.12:GUS* and *pNPF2.13:GUS*. (**C**) Left: Nile red-stained 5-day-old *npf* mutant roots mock

treated or treated with 5 µM GA_3 or 1 µM ABA. Right: Fluorescent intensity relative to Col-0 quantified from a minimum of 8 roots per treatment, 5 endodermal cells per root, n > 40. Statistical significance was assessed using a Dunnett's test (* $p < 0.05$, ** $p < 0.01$, *** $p < 0.001$). (**D**) Root suberin profile measured by gas chromatography-mass spectrometry. The *y*-axis represents relative peak areas following normalization to a C_{32}-alkane internal standard. Right graph indicates for total suberin composition. Data in bars represent the means ± SE of three biological replicates. * indicates statistically significant differences compared with Col-0 at $p \leq 0.015$, ** $p \leq 0.01$ and *** $p \leq 0.001$ by Student's t-test.

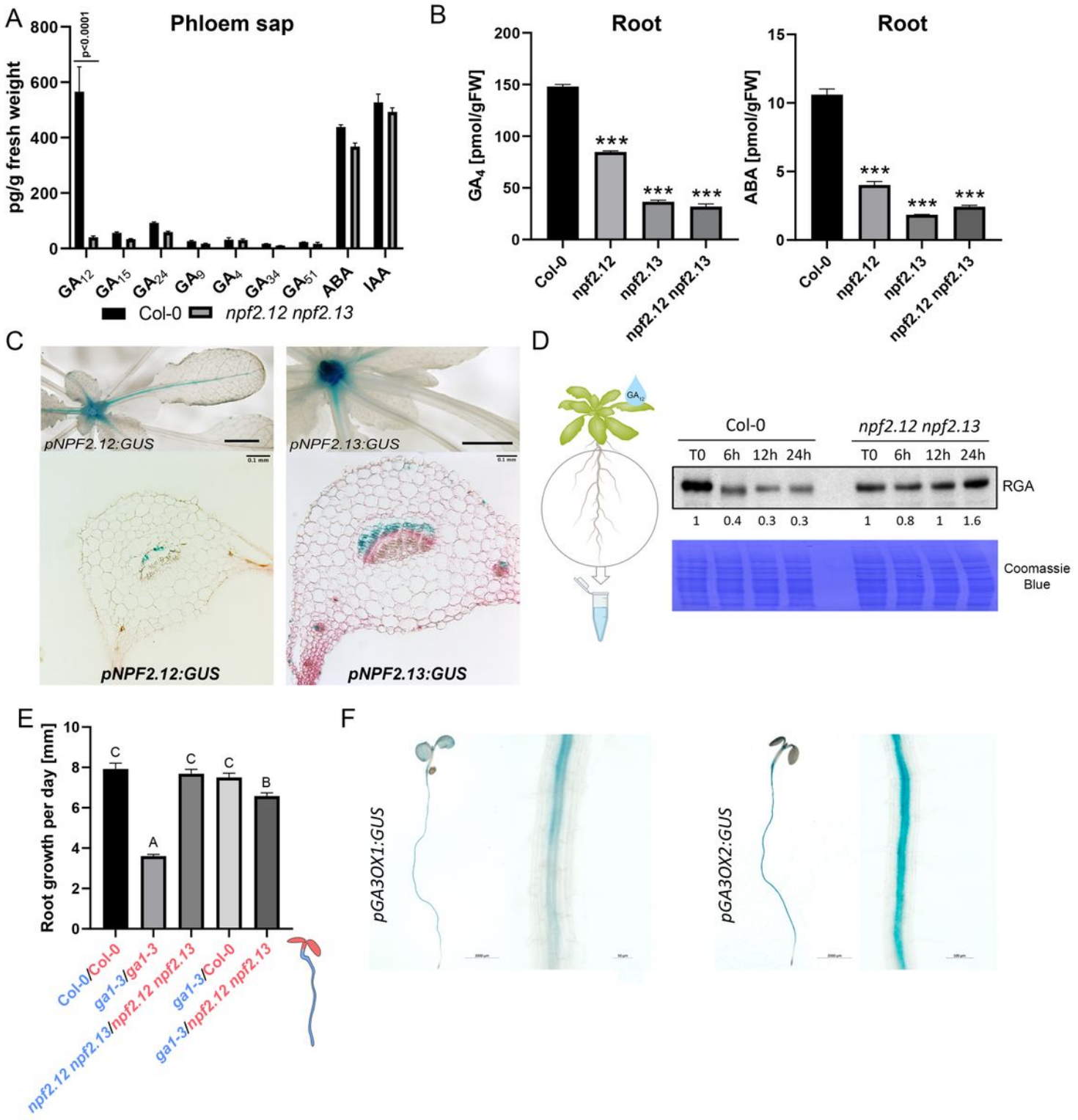

Figure 5

NPF2.12 and NPF2.13 facilitate long-distance shoot-to-root GA transport. (**A**) Quantification of GA, ABA and IAA contents (in $pg.g^{-1}$ fresh weight) in phloem exudates collected from leaf petiole of 5-week-old Col-0 and *npf2.12 npf2.13* mutant plants. Exudate was collected from 75 leaves, pooled into 3 separate biological repetitions (n = 3). Statistical significance evaluated by Dunnett's multiple comparisons test, comparing to Col as control. ($p < 0.0001$) (**B**) GA_4 and ABA quantification (in $pmol.g^{-1}$ fresh weight) in 10-day-old roots of Col-0 and *npf2.12 npf2.13* double-mutant plants (n = 5). Significance was assessed using Dunnett's multiple comparisons test (*** $p \leq 0.0001$). (**C**) GUS staining patterns in rosette leaves of 4 week-old *pNFP2.12:GUS* and *pNPF2.13:GUS* plants. Top images are whole plants; scale bars represent 0.25 cm. Bottom images are cross-sections of GUS-stained leaf petioles; scale bars represent 0.1 mm. (**D**) Immunodetection of RGA protein accumulation in the root of 16-day-old Col-0 and *npf2.12 npf2.13* mutant plants. The plants were grown *in vitro* for 12 days and then moved to MS plates containing a low concentration of nitrogen (0.5 mM KNO_3) and paclobutratol (PAC, 1 µM). 4 days after transfer, a drop of GA_{12} (5 µl at 1 µM) was added to one of the first two leaves formed. Proteins were extracted from the root at 4-time points following GA_{12} application. Similar results were obtained in two independent experiments. (**E**) Root growth (mean ± s.d.; n > 10) of various combinations of grafted seedlings. Blue font indicates for rootstock genotype, red indicates for grafted scion. Different letters denote significant differences ($p < 0.05$) using one-way ANOVA followed by a Tukey's test for multiple comparisons. (**F**) Images of 6-day-old plants that express GUS driven by the *GA3OX1-2* promoters.

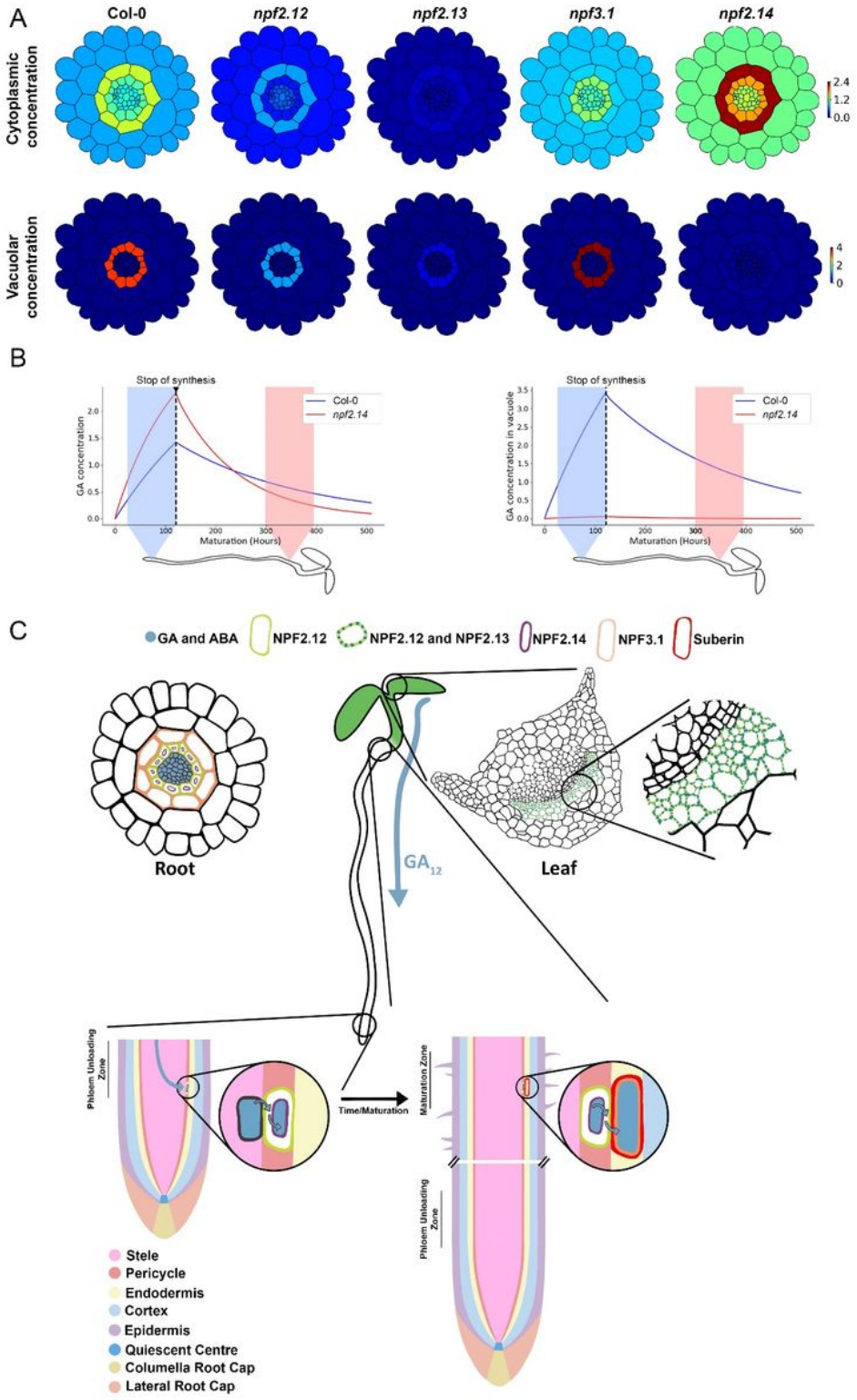

Figure 6

NPF transporters mediate pericycle-specific hormone uptake into the vacuoles at the phloem unloading zone to facilitate a hormone slow-release mechanism that allows suberization at the maturation zone. (**A**) Spatial distributions of cytoplasmic and vacuolar GA concentration in the root cross-section, predicted by the multicellular mathematical model, for the wild type, and the *npf2.12*, *npf2.13*, *npf3.1*, and *npf2.14* mutants. The time of the simulations is 5 days (120 hours), corresponding to the age of the plants used

in the experiments. (**B**) Predicted dynamics of the endodermal cytoplasmic and pericycle vacuolar GA concentration for the wild type and the *npf2.14* mutant. The model is initially simulated with a constant GA source in the stele (pale blue region), then synthesis is set to zero to simulate the GA redistribution after cells leave the phloem unloading zone. The model predicts that NPF2.14 leads to higher endodermal cytoplasmic concentrations where suberin forms (pale red region). (**C**) Proposed model incorporating experimentally observed distributions of root GA transporters, hormone accumulation, endodermal suberin formation and mathematical model predictions. NPF2.12 and NPF2.13, which are localized to the shoot phloem, are both required for GA_{12} long-distance shoot-to-root translocation. NPF2.12 is expressed in the root pericycle cell membranes and promotes the movement of ABA and GA from the vasculature to the pericycle. Once in the pericycle cytoplasm, NPF2.14 imports the hormones into the vacuole to form a reservoir which will be available in later stages. When the root elongates over time and the cells that accumulated high levels of GA and ABA in the vacuoles mature, the hormones are exported out of the pericycle vacuole and imported into the endodermis by NPF3.1 to induce suberization.

Supplementary Files

This is a list of supplementary files associated with this preprint. Click to download.

- SupplementaryMaterial.pdf